Long Coherence Length 193 nm Laser for High-Resolution Nano-Fabrication

June 27, 2008

Sponsored by

Defense Advanced Research Projects Agency (DOD)

MTO

ARPA Order AD63-42

Issued by U.S. Army Aviation and Missile Command Under

Contract No. W31P4Q-07-C-0262

Name of Contractor: Actinix

Principal Investigator: James J. Jacob

Business Address: 229 Technology Circle, Scotts Valley, CA 95066

Phone Number: (831) 440-9388

Effective date of contract: August 2, 2007

Short Title of Work: "Long Coherence Length 193 nm Laser"

Contract Expiration Date: May 27, 2008

Reporting Period: August 2, 2007 through May 27, 2008

REPORT DOCUMENTATION PAGE

Form Approved
OMB No. 0704-0188

PLEASE DO NOT RETURN YOUR FORM TO THE ABOVE ADDRESS.

1. REPORT DATE *(DD-MM-YYYY)*	2. REPORT TYPE	3. DATES COVERED *(From - To)*
27-06-2008	Final	02-08-2007 - 27-05-2008

4. TITLE AND SUBTITLE

Long Coherence Length 193 nm Laser for High-Resolution Nano-Fabrication

5a. CONTRACT NUMBER

W31P4Q-07-C-0262

5b. GRANT NUMBER

5c. PROGRAM ELEMENT NUMBER

6. AUTHOR(S)

James J Jacob

5d. PROJECT NUMBER

5e. TASK NUMBER

5f. WORK UNIT NUMBER

7. PERFORMING ORGANIZATION NAME(S) AND ADDRESS(ES)

Actinix
229 Technology Circle
Scotts Valley, CA 95066

8. PERFORMING ORGANIZATION REPORT NUMBER

9. SPONSORING/MONITORING AGENCY NAME(S) AND ADDRESS(ES)

Director
Defense Advanced Research Projects Agency
ATTN: MTO (Dr. Michael Fritze, Sponsor)
3701 North Fairfax Drive
Arlington, VA 22203-1714

10. SPONSOR/MONITOR'S ACRONYM(S)

DARPA MTO

11. SPONSOR/MONITOR'S REPORT NUMBER(S)

12. DISTRIBUTION/AVAILABILITY STATEMENT

Approved for public release; distribution unlimited.

13. SUPPLEMENTARY NOTES

DARPA STTR Topic 2007-006

14. ABSTRACT

Immersion lithography using available 193 nm optics and laser sources provides an attractive near-term path to reducing the printable feature sizes of integrated circuits by using a high-index fluid to reduce the wavelength at the wafer, rather than using light with higher photon energy and shorter vacuum wavelength. An interferometric immersion lithography (IIL) tool has demonstrated rapid fabrication of grating structures with half-pitches of 35 nm over exposure areas of 0.5 mm. This Phase I project has resulted in the design of a high power, sub-200 nm solid-state light source with very high spatial- and temporal-coherence to allow uniform high-contrast intensity fringes (<30 nm HP) to illuminate a wafer surface over a substantially larger exposure area, on the order of a 22 x 33 mm exposure site. In addition, the laser will have high power stability and be sufficiently robust to allow extended periods of operation with little maintenance or operator intervention.

15. SUBJECT TERMS

nano-fabrication, interference lithography, ultraviolet laser

16. SECURITY CLASSIFICATION OF:			17. LIMITATION OF ABSTRACT	18. NUMBER OF PAGES	19a. NAME OF RESPONSIBLE PERSON
a. REPORT	b. ABSTRACT	c. THIS PAGE			James J. Jacob
U	U	U	UU	55	19b. TELEPHONE NUMBER *(Include area code)* (831) 440-9388

1. Executive Summary

The printing of ultra-fine gratings on silicon wafers using interference immersion lithography is envisaged as a first maskless process step in the low-volume fabrication of advanced application specific integrated circuits. Following the first exposure, critical circuit topographies are made by trimming the grating with an e-beam tool, for example, and then less critical layers are patterned with more conventional wafer processing tools. Substantial economic advantages of this approach are realized in that high cost mask sets and expensive full-blown lithography scanners are not needed. These immersion interference lithography tools will require a new class of laser source that can provide both high spatial and temporal coherence as well as high power to print sub-30 nm gratings over large fields. These coherence requirements are difficult to attain at a low cost with ArF excimer lasers. In this Phase I STTR we have successfully designed and modeled a solid-state laser source that exceeds our target specifications and will accommodate even the most aggressive nano-scaling fabrication strategies.

In 2006 Actinix entered into a joint development with IBM Almaden Research Center to construct a rugged and reliable 193 nm solid-state laser source for IBM's immersion interference lithography tool. This litho test-bed, named NEMO, is used for evaluating photoresists, high index fluids and optical materials in support of next generation immersion lithography. Although this tool represents the state-of-the-art in interference lithography, the laser's moderate bandwidth of 7 pm (56 GHz) limits the grating size it can print to approximately 0.6 mm, assuming a visibility of 90%. Furthermore, the maximum sustained power capability of this laser is about 25 milliwatts, which also limits large field exposures. The laser specifications targeted for Phase I were a bandwidth of less than 3 GHz and an average power greater than 100 milliwatts, enabling exposures of centimeter sized fields. In this final report we describe the design of a single frequency light source with a bandwidth less than 500 MHz and an average power of approximately 250 milliwatts. This laser will have a coherence length on the order of 0.6 meter, one hundred times greater than the NEMO laser and enough power to expose full fields (22 x 33 mm) at sub-30 nm half-pitches. We are also advocating a slight shift in the exposure wavelength to 196 nm for two reasons. First, significantly higher power is attainable due to the increased conversion efficiencies of the non-linear crystals used to generate 196 nm. Second, high index optical materials (like sapphire and LuAG) and higher index next generation immersion liquids have lower optical absorption at 196 nm. Therefore, newly developed second and third generation immersion materials and fluids that are marginally effective at 193 nm potentially will function well at 196 nm allowing the further shrinkage of circuit geometries with interference immersion lithography. We have also verified with resist chemists that the 193 nm ArF photoresists are completely compatible with 196 nm light exposures.

With our research partner, Sandia National Labs (Albuquerque, NM), we have analyzed four laser architectures, shown in Figure 1. Using the SNLO non-linear optics modeling program and new fiber laser models both developed at Sandia National Labs, we were able to analyze pulsed and continuous wave (CW) system architectures. Our conclusion is that the detrimental non-linear effects of self phase modulation and stimulated Brillouin scattering preclude pulsed fiber laser amplifiers from meeting our required power and coherence specifications. While CW fiber laser amplifiers are less susceptible to

these non-linear effects, they present a high degree of technical risk and entail high project costs to develop the complex ultraviolet up-converters for the infrared fiber laser. Therefore our recommended design is based on proven solid-state laser technology with lower development costs and we have a high degree of confidence of developing a quality interference lithography light source in a Phase II project.

System Description	System Architecture	Comments
A. Pulsed dual fiber laser: 193 nm • 938 nm Nd and 1103 Yb nm fiber laser front ends • 1 ns pulses; 20 MHz PRF • PPLT frequency doubler (469 nm) • DUV @ 234.5 nm: 10 crystal BBO freq. doubler • 193 nm mixer: CLBO	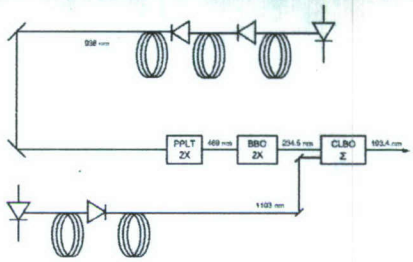	**Advantages:** • All fiber laser front end • 20 MHz PRF is quasi – CW: applicable to wafer inspection **Disadvantages:** • 938 nm Nd fiber laser unproven • BBO absorbs DUV • Highly complex DUV generation scheme
B. Pulsed fiber laser/OPO: 195 nm • 1080 nm fiber pump laser • PPLT doubler (540 nm) • OPO @ 950 nm (PPLT) • PPLT doubler (475 nm) • DUV @ 237.5 nm: CLBO • CLBO mixer	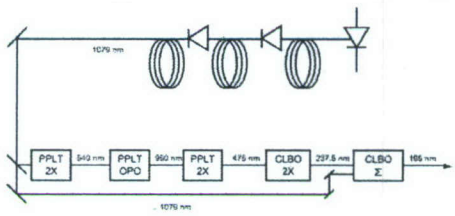	**Advantages:** • Single fiber laser front end **Disadvantages:** • Self-phase modulation: 1 ns fiber pulses needed to get 3 GHz bandwidth • OPO marginal with sub-ns pump pulse
C. CW Fiber Laser/OPO: 195 nm • CW fiber laser front end • 4 resonant enhancement cavities + CW OPO cavity • CLBO DUV @ 237.5 nm • CLBO 195 nm mixer	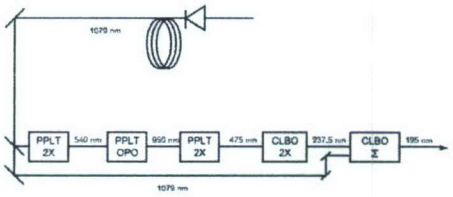	**Advantages:** • Single fiber laser front end • CW operation **Disadvantages:** • Many resonant cavities • High development cost • Limited average power
D. Pulsed Laser/OPO: 196 nm • Injection seeded pump laser • BiBO OPO (seeded) • DUV 240 nm CLBO mixer • 196 nm CLBO mixer	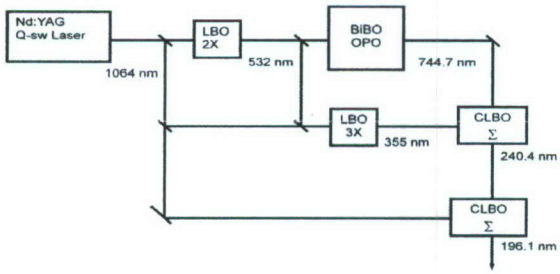	**Advantages:** • Extension of proven laser technology • Low development costs • High average power • Long coherence length **Disadvantages:** • 5 KHz not applicable to wafer inspection

Figure 1: The four sub-200 nm laser architectures studied in the Phase I effort. Show-stoppers are indicated in red. The candidate architecture for Phase II is system D, the pulsed OPO system operating at 196 nm.

2 .Phase I Objectives

The overall technical objective outlined in the Phase I proposal was to identify, design, and model an optimum combination of fiber laser and nonlinear conversion stages that would result in a high-power, narrow-bandwidth 193-nm laser source suitable for a low-volume manufacturing interference immersion lithography tool. We studied a number of fiber systems and concluded that this particular technology is not well suited to the generation of long coherence light in the far ultraviolet because of non-linear effects that are inherent in the fiber physics. Instead we have chosen a solid-state laser approach to address this application. This system exceeds the proposed specifications and is an economical approach to this problem. The key tasks and results of the Phase I work are summarized as follows:

a. Identification of candidate fiber laser systems

Fiber systems were identified that had the proper wavelengths to allow conversion to the far ultraviolet, less than 200 nm. We studied two types of fiber systems: a Nd doped fiber that operates in a quasi-three level mode, having a gain peak at 938 nm, and Yb doped fibers operating over the range from 1070 nm to 1105 nm. We also identified a solid-state diode pumped laser as an alternative approach to achieving the simultaneous requirements of long coherence length and high average power.

b. Design fiber laser/amplifier stages

Three fiber architectures (see Figure 1) were modeled using software developed by our research collaborator Dr. Arlee Smith at Sandia. We also modeled and designed a light source using solid-state laser based technology as discussed throughout this report. The ultimate design is based on an injection seeded solid-state q-switched Nd:YAG laser with extremely long coherence length. The seeded Nd:YAG laser has a bandwidth of typically 90 MHz.

c. Design nonlinear conversion stages

We designed the various non-linear optical stages involving the selection of the specific crystals in the non-linear optical up-converter, as well as specifying their interaction lengths, phase-matching angles, coatings, temperatures of operation and beam parameters for optimum conversion efficiency

e. Model overall performance of combined fiber/nonlinear converter

The fiber systems are discussed briefly in section 6. More details of the fiber modeling and analysis work are given in the appendix. The solid-state196 nm laser system is discussed in detail in section 7. Our candidate design for Phase II provides for an average power capability of approximately 250 mW with a bandwidth less than 0.5 GHz. The possibility of further power scaling brings the potential to print full fields (22 by 33 mm) in exposure times of less than one second.

3. Laser Requirements for Interference Lithography Tools

A schematic diagram of the IBM NEMO interferometer head is shown in Figure 2. An interference lithography tool incorporates a variety of optics to combine two beams of collimated 193 nm light, at high angles, at the surface of a silicon wafer that is in contact with a layer of an immersion fluid. The period of the interference grating produced at the surface of the resist is given by $\lambda/2n \sin(\theta)$, where λ is the wavelength of the illumination, 2θ is the full angle between the interfering beams, and n is the index of refraction of the liquid layer. The angle of incidence of these beams on the wafer is controlled by the geometry of a fused silica prism with its bottom surface parallel to and just above the wafer, and also in contact with the immersion fluid.

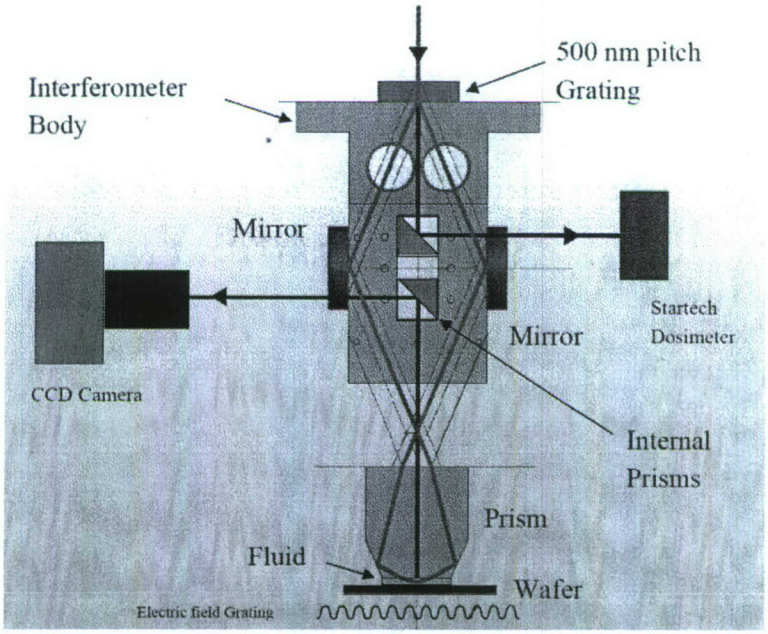

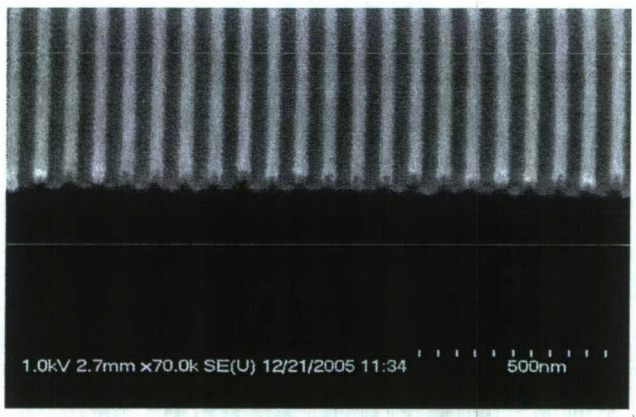

Figure 2: ***Upper*** - Schematic diagram of the IBM NEMO interferometric immersion lithography test stand. Prisms produce periodic intensity maxima spaced by 70, 80 or 90 nm (giving grating lines 35, 40 or 45 nm wide respectively). ***Lower*** – SEM image of 35 nm half-pitch lines/spaces printed on NEMO with the Actinix 193 nm laser.

An interference lithography laser light source must provide a very highly spatially- and temporally-coherent beam. A high degree of spatial coherence is necessary to provide uniform (i.e., straight) grating patterns with minimal aberration or chirp. The temporal coherence-length of the illumination source determines the field sizes that may be reliably patterned for a given grating half-pitch. Physically, when optical path differences between interfering beams become comparable to the temporal coherence length of the source, the fringe contrast diminishes, ultimately washing out the grating structures. From geometric arguments, it can be shown that the path difference between the interfering beams depends on the relative angle at which they interfere, and so for a fixed field size, the patterning of increased pitch density structures (reduced half-pitches) requires longer source coherence length. The effect of temporal incoherence is that the fringes generated by the interferometer have perfect modulation only on the exact centerline of the prism; as one moves away from the centerline the modulation depth of the aerial image becomes progressively smaller. This is demonstrated by the SEM images in Fig. 3 of an exposure that used a 70 nm thick layer of JSR AR1682J photoresist on an AR24 antireflection underlayer (Rohm and Haas Electronic Materials) with a JSR TCX014 topcoat on a 125 mm silicon wafer. Fringes of 90% visibility are formed in a strip 0.6 mm wide when using the laser with a 7 pm spectral bandwidth.

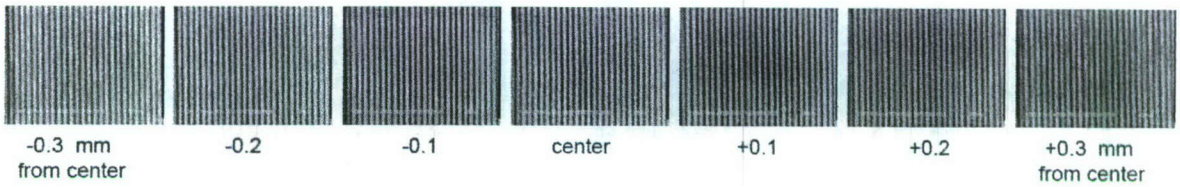

Figure 3: SEM images of 35 nm half-pitch features produced using the IBM NEMO interference litho tool. Note pattern degradation occurring ~0.3 mm to either side of the center.

A plot of the predicted fringe visibility as a function of the displacement from the centerline of a water immersion interferometer is shown in Fig. 4. The model assumes a laser with a 5 mm coherence length, corresponding to a bandwidth of 7 pm FWHM. The 90% visibility point is 0.3 mm from the centerline.

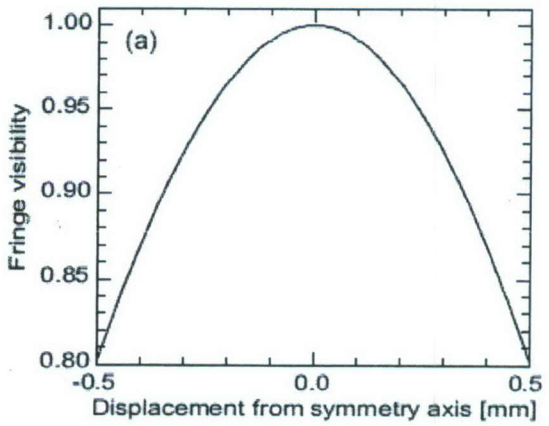

Figure 4: Modeled performance of the NEMO interferometer with the 70 nm pitch prism, assuming that the light source has a Gaussian spectrum with a 7pm FWHM (Courtesy John Hoffnagle, IBM)

To increase the field size we need to increase the coherence length of the laser (reduce its bandwidth). Figure 5 indicates the tradeoffs between desired grating pitch and field size as they relate to the laser spectral bandwidth. The upper three curves in Figure 5 show the finer nano-scale geometries that can be attained when a higher index immersion liquid is used, with a concomitant increase in prism refractive index. For example, water with an index of 1.44 is well matched with a fused silica prism and features down to 35 nm are printable (blue curve). Increasing the fluid index to 1.64 and using a higher index prism material such as crystalline quartz, 30 nm features are possible (red curve). Finally, if a third generation fluid with an index of approximately 1.88 is developed then a prism made of sapphire could be used to fabricate gratings approaching 26 nm half-pitch (green curve).

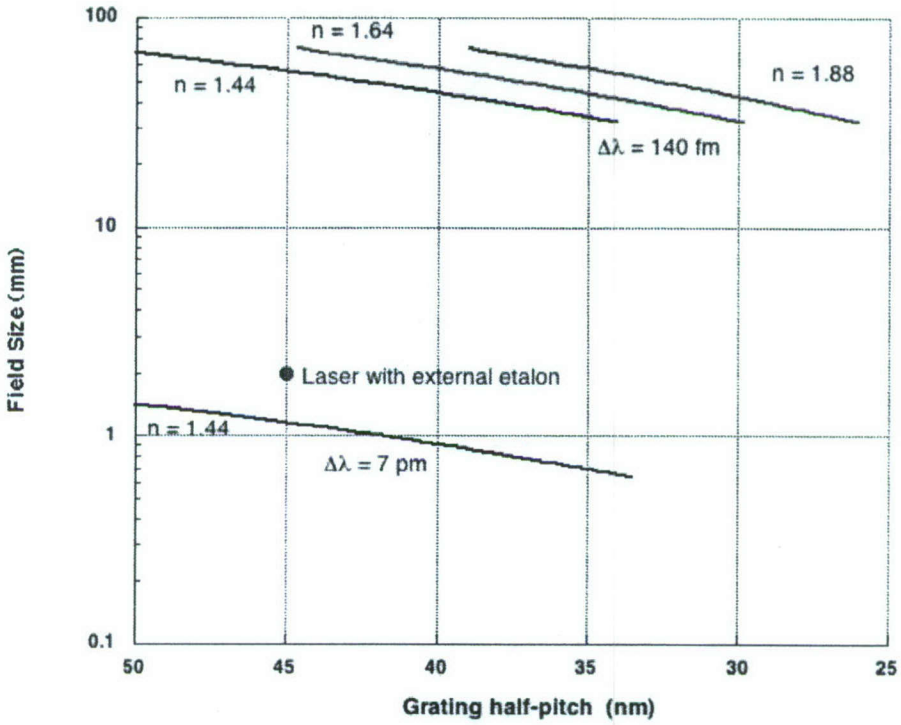

Figure 5: The parameter space of immersion interference lithography assuming 90% visibility. The 193-nm laser with $\Delta\lambda$ = 7 pm in the NEMO tool using water (n =1.44) printed approximately 35-nm half-pitch gratings over a 0.6-mm field. An external etalon ($\Delta\lambda \sim 1$pm) allows 2 mm fields at 45 nm half-pitch in water. Upper curves show field sizes with high index fluids and a 196 nm laser with $\Delta\lambda$ = 140 fm. Expected bandwidth of new laser is $\Delta\lambda$ < 70 fm.

It should be mentioned that IBM now routinely uses an external air-spaced etalon to reduce the laser bandwidth from 7 pm FWHM to about 1 pm, thereby allowing larger gratings to be printed. The etalon is placed directly at the laser output and rotated approximately one milliradian from normal incidence. The average power into the NEMO tool is approximately 2.5 milliwatts. The beam is allowed to propagate without further attenuation into the NEMO apparatus. Using the 45 nm half-pitch prism, 2 mm long grating exposures are made in less than 0.5 second with approximately 2.0 milliwatts average power at the wafer surface. At a 5 kHz pulse repetition rate this corresponds to a wafer exposure dose of approximately 32 mJ per square centimeter, which we believe is at the high end for a typical resist.

The external etalon has two major drawbacks: first, the transmission through the high finesse etalon is quite low, about 12 %, so the laser output power of 20 milliwatts is lowered to 2.5 milliwatts; second, the spectral shape of the etalon filter is not Gaussian, like the light source, but Lorentzian, which is characterized by long wings that tend to degrade the grating contrast. Therefore even though the etalon reduces the laser bandwidth appreciably, the benefit is greatly diminished in terms actual field size improvement due to the presence of this residual optical power in the wings of the spectrum.

What power will be needed to expose larger gratings? To first order, a one-centimeter field would require 25 times the power used on the 2 mm field exposure, or 62.5 milliwatts average power. However, we need to also consider the beam uniformity. These solid-state lasers have Gaussian beam profiles; therefore truncation is required to flatten the field which means a large fraction of the light is discarded. For example, specifying 10% uniformity across the field (a variation of +/- 5%) requires truncating 90% of the Gaussian profile and losing 90% of the power. Thus a one-cm field requires a 625 mW source (at a 32 mJ/cm^2 exposure). Extending the exposure time to one second would lower the power requirement to 312 mW. There is an optical solution to this problem: Gaussian to flat-top beam converters. These are aspheric lens pairs that convert the Gaussian to a top-hat profile with the same 10% variation but with just a 30% loss. A one square centimeter field would then require about 90 mw, assuming the same dose in 0.5 second. If one considers that our proposed laser will deliver 250 milliwatts and the coherence length is one-half meter, then the possibility arises of future interference tools printing full fields (22x33 cm) at doses of say 15 mJ/cm^2 with one-half second exposure times.

We have made reference to the advantages of operating the immersion litho tool at 196 nm. We show here in Fig. 6 a trace of the absorbance of an early generation-2 fluid. Note the steep slope in the vicinity of 193 nm. Newer fluids have lower absorbance but the same spectral shape with the transmission at 196 nm about twice that of 193 nm. This can have profound effect on fluid heating and lifetime. We also are investigating the transmission characteristics at 196 nm of prism materials like sapphire and LuAG.

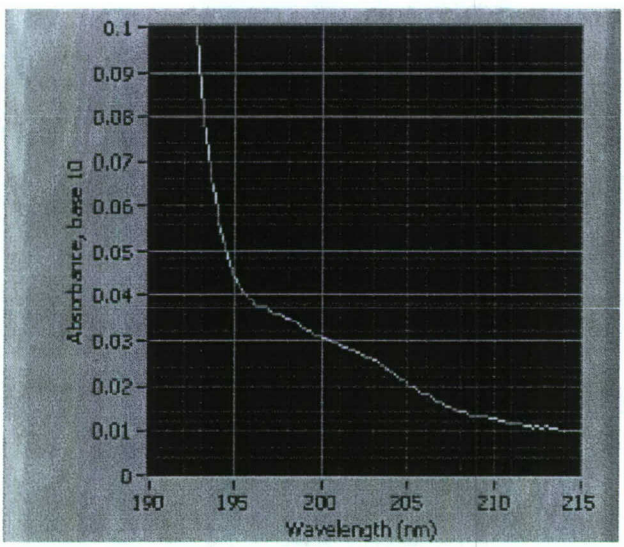

Figure 6: Absorbance spectrum of an early generation 2 fluid near 193 nm (Courtesy V. Liberman, MIT Lincoln Labs)

4. Laser Coherence Length and Bandwidth

We now briefly discuss the relation of laser spectral bandwidth to coherence length and the measurement method used. A Michelson interferometer was used to directly measure the coherence length of the 193-nm laser installed in the IBM NEMO tool. The principles of this procedure, wherein the fringe contrast or visibility of a two-beam interferogram is measured for a variety of optical path-length differences (OPD), are well known. As the OPD of the interferometer arms is varied, one sees a variation in the fringe visibility, which depends on the spectral composition of the source.

Figure 7 shows CCD images of 193-nm fringe patterns obtained at two different OPD values used in this coherence length measurement. The fringe visibility for the interferogram of Fig. 7(a), with zero OPD, is 0.952, whereas for Fig. 7(b), with a 1-mm mirror translation, it is 0.46. The fitted fringe visibility V is plotted as a function of the position of the movable mirror (relative to an arbitrary origin). The visibility has a Gaussian dependence on the length of the interferometer arm, as shown by the solid curve.

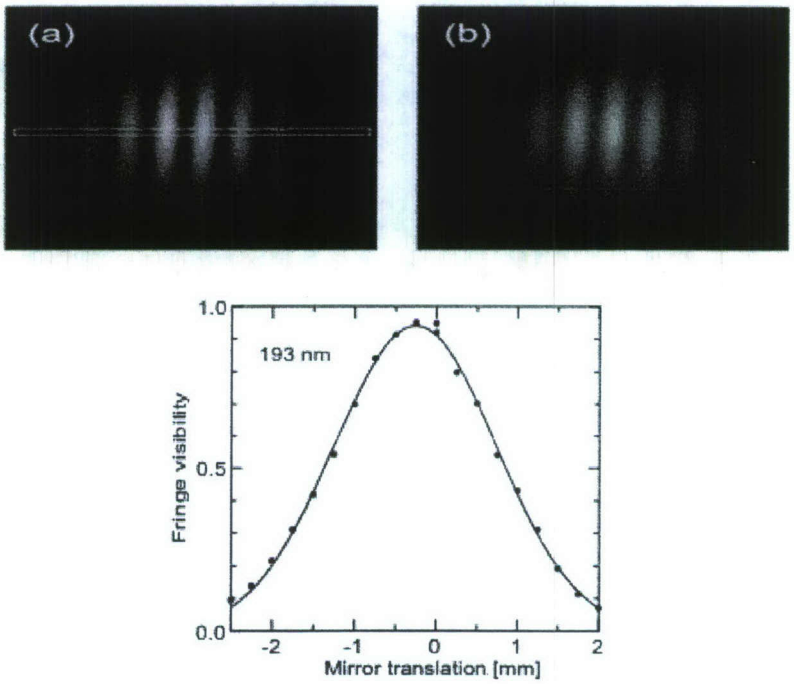

Figure 7: Fringe visibility when one mirror of the Michelson interferometer is translated. Points are measured visibility from fits to the measured fringe patterns. Solid line is a Gaussian function. (Courtesy John Hoffnagle, IBM)

The standard deviation of this curve is 0.991 mm; since the optical path length difference is twice the mirror displacement, the visibility expressed as a function of optical path difference has a standard deviation

$$\sigma_s = 1.982 \text{ mm}.$$

The Gaussian fringe visibility curve leads to a Gaussian spectral line shape given by

$$f\,(k) = \frac{1}{\sqrt{2\pi}\sigma_k} exp\left(-\frac{k^2}{2\sigma_k^2}\right)$$

where,

$$\sigma_k = \frac{1}{\sigma_s}$$

The FWHM bandwidth expressed in wavenumbers is

$$\Delta_k(FWHM) = \frac{\sqrt{2ln2}}{\pi}\sigma_k = 1.9cm^{-1}$$

Expressed in frequency units with 1 cm^{-1} = 30 GHz,

$$\Delta_\nu\,(FWHM) = 56.4\,GHz.$$

In terms of wavelength, the spectral line shape is also Gaussian with a standard deviation of

$$\sigma_\lambda = \frac{\lambda^2}{2\pi}\sigma_k$$

The full width at half maximum (FWHM) as a measure of line width is given by

$$\Delta\lambda\,(FWHM) = 2\sqrt{2ln2}\sigma_\lambda$$

Using these relations with our measured data implies

$$\Delta\lambda\,(FWHM) = 7.04\,pm$$

The coherence length is then given as:

$$L_c = {\lambda^2}/{\Delta\lambda}$$

$$L_c = 5.3\,mm$$

Table 1 is a summary of the spectral characteristics for the lasers discussed in this report.

Laser Specifications	Bandwidth (GHz)	Bandwidth (pm)	Bandwidth (cm^{-1})	Coherence Length (cm)
NEMO	56.4	7.04	1.9	0.5
Phase I goal	3.0	0.37	0.10	10
Phase II projection	0.5	0.06	0.016	62

Table 1: Spectral specifications (FWHM values) of the laser currently in use, of the laser originally proposed for Phase I, and of the laser architecture to be developed in Phase II.

5. Sub-200 nm Solid-state Laser Design Considerations

Generally the preferred approach to making sub-200 nm light using solid-state laser technology is to begin with an infrared laser then up-shift its frequency to the ultraviolet with a network of non-linear crystals. One example is to generate an intermediate frequency in the deep ultraviolet (DUV), say from a harmonic of the infrared laser, then sum-frequency mix the DUV radiation with a tunable oscillator in the near infrared, thereby allowing some wavelength selectivity at the target wavelength. The patented Actinix 3193 laser system depicted in Figure 8 uses this concept. A q-switched, intracavity frequency doubled Nd:YAG laser drives an optical parametric oscillator (OPO) running at 710 nm. A portion of the 532 nm light is doubled in a CLBO crystal to 266 nm. These wavelengths are subsequently summed to generate 193 nm in a 7 mm long BBO crystal. The benefits of this design are that it only requires three crystals following the pump laser and it can provide a moderate power level of up to 25 milliwatts.

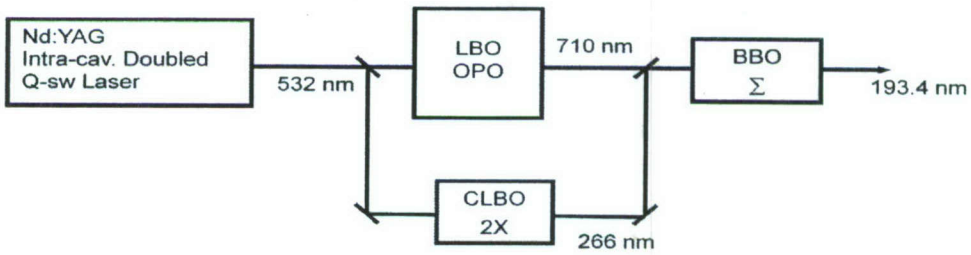

Figure 8: Schematic of the Actinix 3193 laser developed for the IBM NEMO tool.

The intracavity doubled, q-switched Nd: YAG laser provides 15 ns long pulses each with 2.5 mJ energy at a 5 kHz pulse rate. It has an excellent spatial mode. When doubled in CLBO its spectral bandwidth is on the order of 1.8 cm^{-1} at 266 nm. The 710 nm OPO uses for its output coupler a volume Bragg grating mirror, resulting in a bandwidth value of about 0.6 cm^{-1}. These bandwidth values fall within the acceptance bandwidths of the BBO crystal for this particular interaction. The output bandwidth at 193 nm is driven primarily by that of the 266 nm wave which is difficult to decrease because the intracavity doubled Nd:YAG laser is optically complex and not amenable to standard line narrowing methods.

A second limitation of this 193 nm source is the difficulty in scaling its power beyond 25 milliwatts due to the fact that the final BBO mixing crystal is highly absorptive to radiation at wavelengths below 200 nm. The BBO crystal in the Actinix 3193 system is actually cooled to minus 30 degrees C with a four-stage thermo-electric device that itself is water cooled. Using this apparatus we were able to reduce the absorption at 193 nm from 0.14/mm to 0.08/mm. As a result the average power increased by a factor of three over the room temperature operation. Still the BBO crystal witnesses a substantial amount of 193 nm loss to linear absorption. This loss of course is converted to heat which then further detunes the crystal phase-matching by altering the indices of refraction with the rise in temperature.

For higher average powers at a wavelength less than 200 nm, there is only one commercially available crystal that has the necessary combination of low optical absorption and favorable non-linear optical properties: CLBO (cesium lithium borate). However, CLBO is extremely hygroscopic so operating it at an elevated temperature of around 150 degrees centigrade is imperative. Otherwise it is an excellent

material for far ultraviolet light generation. It serves as the frequency quadrupler (266 nm) in the Actinix 3193 and has been running at IBM for nearly two years with no downtime. So the crystal can be quite robust if operated continuously at elevated temperature.

This constraint in operating the CLBO specifically at 150 degrees C determines the allowable interacting intermediate wavelengths that can generate ultraviolet wavelengths at the far end of the crystal transparency range. The ordinary and extraordinary indices of refraction are functions of the crystal temperature and thus the k-vectors for the particular three-wave interaction are as well. The tuning in this region is extremely critical and rapid, where a fraction of a degree in temperature or a slight shift in wavelength will push the crystal beyond the allowed phase matching region. In Figure 9 we indicate the input wavelengths required for sub-200 nm generation using sum-frequency mixing in non-critically phase-matched CLBO operating at 150 C.

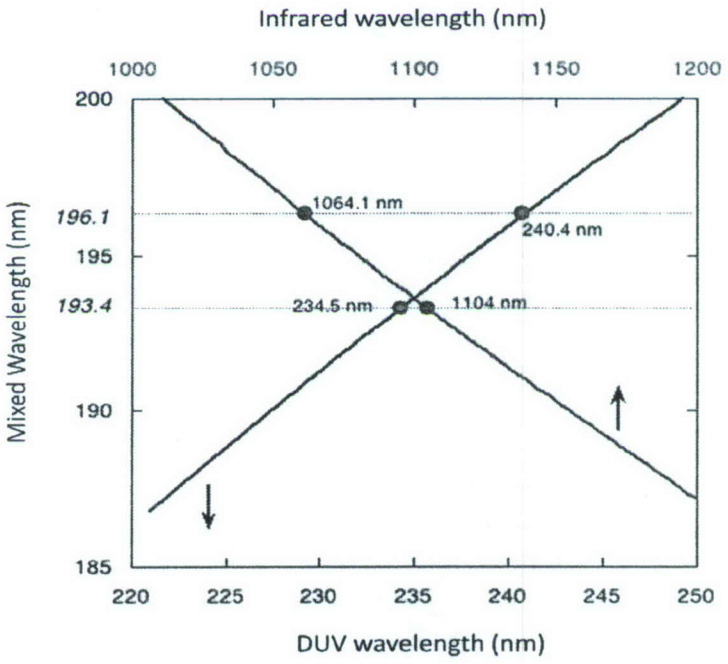

Figure 9: Wavelengths that satisfy sum-frequency non-critical phase-matching conditions in CLBO operating at 150 degrees C. Dashed lines intersect the pairs of DUV and IR wavelengths needed to generate 193.4 and 196.1 nm.

For the highest power operation it is desirable that both the DUV wave and the 193 nm output are generated in CLBO. The phase matching boundary conditions of CLBO however conspire against doing this. The shortest DUV wavelength that CLBO (at 150C) can generate as a second harmonic wave is 237.5 nm. The longest DUV wavelength that CLBO (at 150C) can phase-match to generate 193.4 nm is 234.5 nm. Therefore something has to give, either lowering the CLBO temperature (which is forbidden) or changing the generated wavelength. We identified the case where 196.1 nm can be generated in CLBO by mixing 1064.1 nm with 240.4 nm. This then allows CLBO to be used in both ultraviolet stages and is the other reason we chose this longer wavelength for our final design.

6. Fiber Lasers Analyzed in Phase I

A. Pulsed dual- fiber 193 nm system

Our initial inclination in designing the long coherence sub-200 nm light source was to utilize fiber laser technology, as rapid progress was reported in the literature and a range of powerful fiber laser products are now commercially available. Large mode area fiber amplifiers promised to deliver high pulse energies at a relative low cost. Not clear to us though were the temporal coherence and pulse energy limitations of fiber amplifiers that were seeded by narrowband signal sources. This particular mode of operation was not well documented before we undertook this project, but as a result of this Phase I work with our Sandia collaborators we now understand this problem quite well.

Our research commenced with searching for a fiber laser solution that could provide enough pulse energy in a bandwidth sufficiently narrow to meet our initial design goal of achieving an average power of 100 mW at 193 nm with a bandwidth of 3.0 GHz. The final bandwidth requirement sets a maximum allowable frequency bandwidth for the infrared front end laser amplifier at approximately 2 GHz, as the subsequent mixing and harmonic converters will tend to broaden the spectrum to 3.0 GHz. The general boundary conditions for narrowband pulsed fiber amplifiers are shown in Figure 10 from a recent paper by Arlee Smith and co-workers. Our system is basically constrained to operate underneath the lines shown that delineate the thresholds for self phase modulation (SPM) and stimulated Brillouin scattering (SBS). The SPM threshold criterion is a doubling of the input linewidth to a value of 1 GHz, thus it approximates our situation. The preferred pulse duration according to this analysis is approximately 1ns.

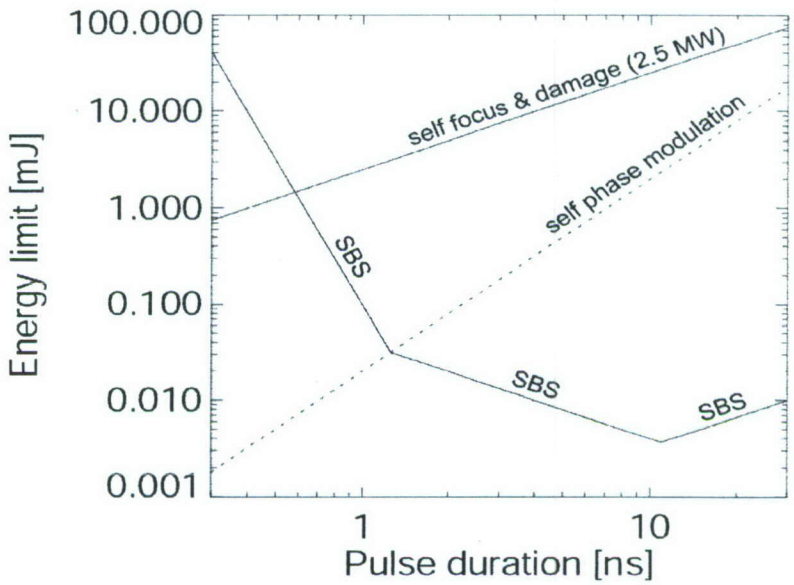

Figure 10: Schematic of energy threshold for each nonlinear process as a function of pulse duration. In our case we are bounded by self phase modulation and SBS. The maximum attainable energy before the spectrum becomes broadened significantly is about 30 microjoules occurring with a one nanosecond pulse width. At longer pulse durations SBS dominates. (A.V. Smith, G.R. Hadley, R.L. Farrow, B.T. Do, CLEO paper CFR2, 2008)

The system shown in Fig. 11 was our initial choice of system architecture for this application since both the UV and infrared mixing wavelengths are derived directly from fiber lasers and there is no need for an intermediate tunable oscillator. This configuration also operates at megahertz pulse repetition rates, thus it could serve in applications like semiconductor inspection that require continuous wave (CW) or quasi-CW lasers for the rapid scanning of wafers for defects. In its favor, this system uses CLBO for the final mixing stage, and because of the particular choice in fiber laser wavelengths, the CLBO can be non-critically phase matched at the required operating temperature of 150 degrees centigrade.

This system employs two seeded fiber amplifiers: the first is a quasi three level Nd doped fiber that provides gain at 938 nm; the second is a Yb doped fiber with gain at 1103 nm. The concept we considered here for each amplifier was to begin with a single frequency CW laser then chop it at a high pulse repetition rate with a semiconductor optical amplifier (SOA) which can be switched extremely fast. The single frequency pulses could then be tailored for the desired pulse duration to be injected into the fiber amplifiers. The bandwidth would be determined by the spectral broadening in the fiber amplifiers. The first fiber amplifier is a quasi-three level Nd doped fiber system that provides gain at 938 nm. Figure 12 shows the modeled spectral broadening due to SPM of the 938 nm fiber amplifier.

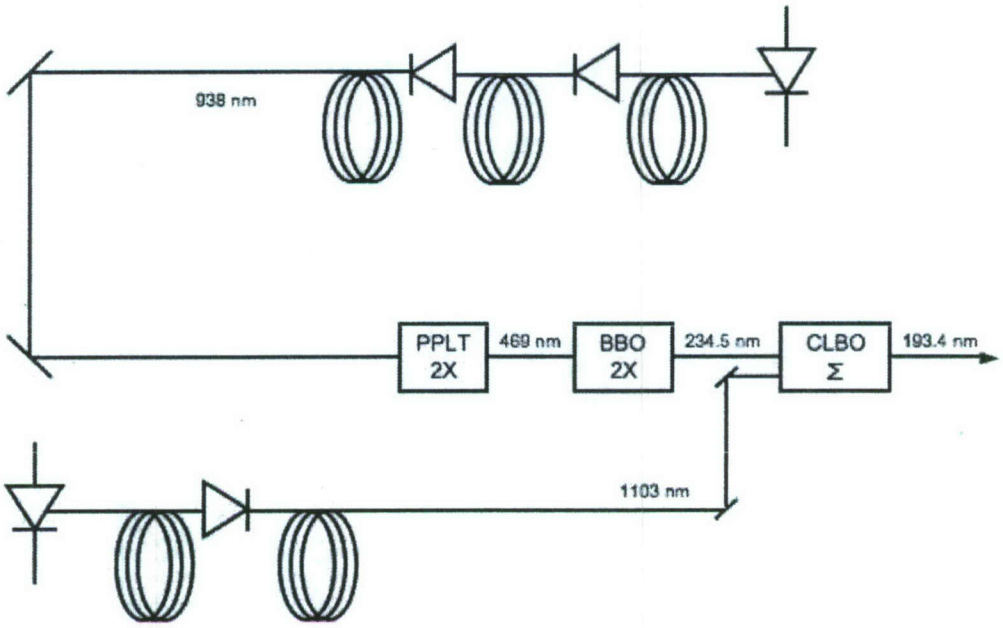

Figure 11: Dual fiber laser architecture: The 938 nm Nd fiber laser when quadrupled provides an intermediate DUV wavelength 234.5 nm. The 1103 nm input to the CLBO mixer is provided directly from a second Yb fiber laser.

The spectrum shows a slightly broader profile than we would like for the reason of keeping the IR bandwidth narrow as the downstream non-linear optics will broaden the spectrum, as mentioned earlier. However, the show-stopper came from the DUV generation stage (the 234.5 nm module). The second harmonic limit for CLBO at 150 C is 237.5 nm, thus BBO is the only choice. Although not as critical as the sub-200 nm generation case, we knew that BBO had issues at the longer 234.5 nm DUV

wavelength as well, but we thought we could possibly engineer a solution to mitigate the absorption and walk-off effects. Unfortunately the solution to achieve this was quite complex in that it required ten crystals. It was based on the concept of distributing the heat load over a series of thin crystals and overcoming the double refraction by orienting the ten crystals in a walk-off compensating configuration. Although entirely feasible on paper, this design was considered too risky to manufacture and to keep aligned over sustained periods of operation. Another issue with this fiber system is that the 938 nm fiber is not a commercially available product.

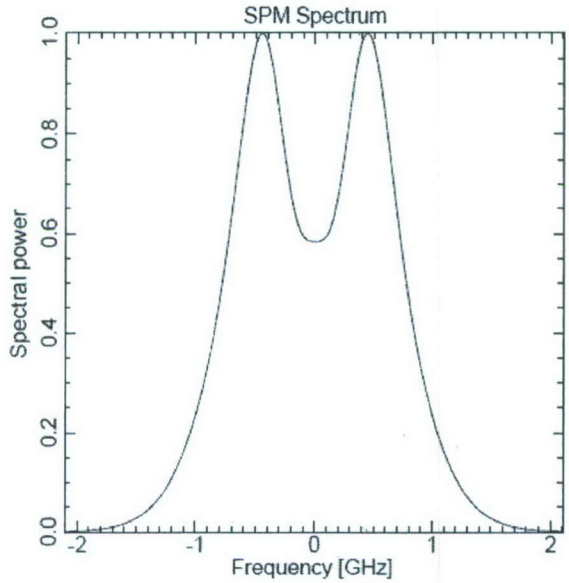

Figure 12: Output spectrum of the final stage 938 nm fiber amplifier

B. Pulsed fiber laser/OPO

The system shown in Figure 13 presents an effort to replace BBO with CLBO for the DUV generation stage. The issue here is that there are no known fiber systems that operate at 950 nm which is the wavelength we need to generate 237.5 nm via quadrupling. Here we consider generating the 950 nm near-infrared wavelength with an OPO, pumped by the second harmonic of an Yb fiber laser system running at 1079 nm. The final output wavelength in this case was 195 nm. The OPO output is doubled twice, first to the blue in periodically poled lithium tantalate, then to the DUV in CLBO. The infrared input to the mixer is supplied by the Yb laser fundamental wavelength.

Again we were constrained to 1 ns pulse durations due to SPM-SBS. Pulsed fiber lasers are not ideally suited to this application because it is difficult to saturate their gain over a sufficient length of fiber to obtain the needed pulse energy without also spectrally broadening the pulse beyond that required to provide a 3 GHz bandwidth at the output wavelength. Pumping the OPO places more burden on the fiber front end than in the previous system because the OPO requires a relatively high energy to work well and it really functions best with pulse durations on the order of 10 ns, beyond the limit where SBS will take over. For these reasons this design was rejected for this application.

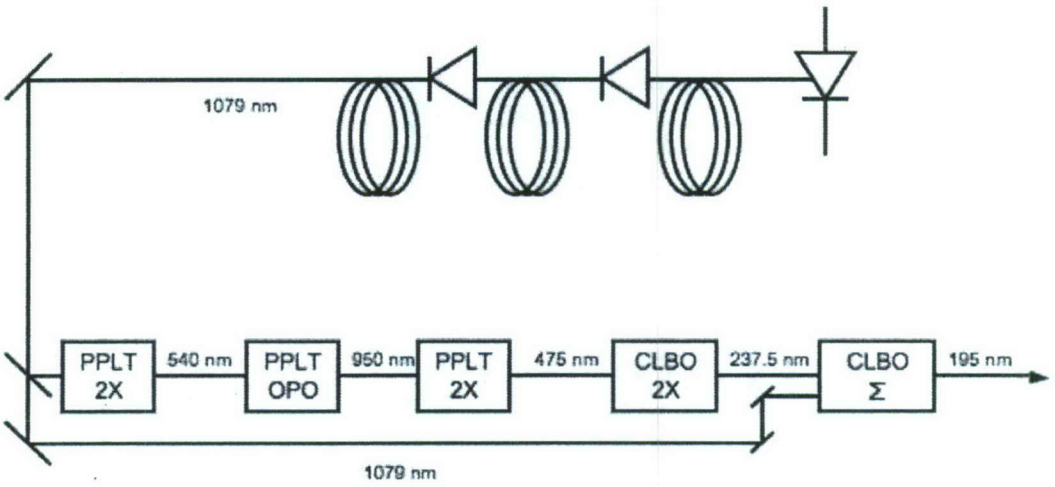

Figure 13: Pulsed fiber/OPO configuration

C. CW fiber system

The CW fiber-pumped system outlined in Figure 14 seems feasible, although it is complex, requiring several stages that use build-up cavities. A power of approximately 20 W from a 1080 nm fiber is sufficient to generate 100 mW at 195 nm. Roughly, 5 W is used to pump the OPO line that produces 100 mW of 238 nm light, and 10 W is used in the final mixing stage that sums 238 and 1080 nm beams. There are four and possibly five resonant cavities required, but these can all be based on a common design and can use common locking electronics. A high beam quality is maintained over the full chain by the resonant cavities, so the 195 nm beam should be high beam quality, and it should also have a narrow spectral linewidth. The build-up cavities have critical mirror coating requirements that usually require multiple runs to optimize. The long wavelength of the fiber is a risk issue as well. The overriding reason we rejected this idea is the high cost of developing the technology.

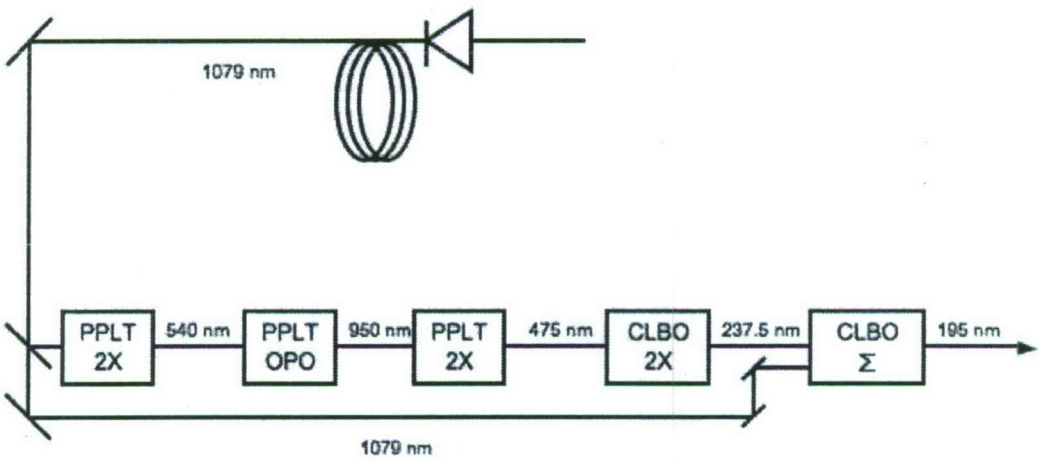

Figure 14: CW fiber system architecture

7. Long Coherence Length Solid-state 196 nm Laser

The system shown in Figure 15 is the laser architecture we are proposing for the pending Phase II project. It is based on a solid-state laser and OPO similar to the Actinix 3193 light source developed for the NEMO tool but adapted to employ CLBO in the DUV and final mixing stages. In this system we are not utilizing an intracavity doubled Nd:YAG laser, rather we are externally doubling the infrared laser. There are two reasons for doing this. First, the pump laser will be injection seeded with a single frequency Nd fiber laser. The intracavity doubled lasers are not amenable to injection seeding because of their complex optical construction. Second, we are using the 1064 nm fundamental wave to triple to 355 nm and as an input to the final mixing stage, so we need access to it. A preliminary light budget is presented in Table 2, showing the optical powers at the various stages in the process and the characteristics of the particular crystal used at each stage.

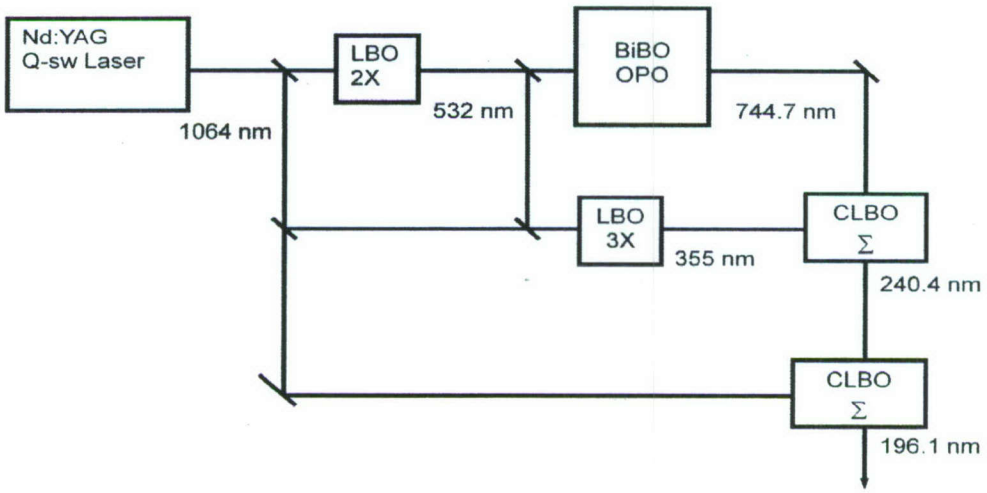

Figure 15: Architecture of high power, long coherence length solid-state 196 nm laser

Nd:YAG Laser

The Nd:YAG laser is a commercially available diode-pumped q-switched Nd:YAG laser that provides up to 20 watts of average power at 10 kHz repetition rates. The pulse duration is 40 ns. The Model DS20-1064 from Photonics Industries (Bohemia, New York) is one possible commercial product we can use as the main infrared source for the system. We will probably buy the laser and then add the injection seeder ourselves, although the Nd:YAG laser vendor may also provide an integrated injection seeded solution. Injection seeding technology has improved greatly with the advent of single frequency fiber lasers that can provide high wavelength stability, output powers in excess of 100 mW and linewidths less than 10 kHz (for example the Scorpio form NP Photonics, Tucson, AZ) . The injection seeder narrows the bandwidth of the q-switched Nd:YAG laser to approximately 90 MHz (0.003 cm^{-1}). We plan to lock the Nd:YAG q-switched laser to the fiber laser master oscillator by using the build-up time reduction method, in which the time delay from the opening of the q-switch to that of the pulse leaving the cavity is monitored and minimized by adjusting the cavity length of the slave laser.

Wavelength	Average power	Pulse energy	Pulse duration	Crystal NL coeff	Crystal length	Walkoff angle	Beam dia	Gain medium
λ	P	E	Δt	d_{eff}	L	ρ	d	
nm	W	mJ	ns	pm/V	mm	mrad	μm	
196.1	0.308	0.031	18	1.1	15	0	250	CLBO
240.4	0.375	0.038	20	0.9	15	27	250	CLBO
355	1.5	0.150	25	0.73	30	17	300	LBO
744.7	1.0	0.10	20	2.46	15	5.6	250	BiBO
532	10	1.0	28	0.6	35	0	150	LBO
1064	20	2.0	40					Nd:YAG

Table 2: The estimated light budget of the long coherence length 196-nm system calculated from SNLO models. This preliminary analysis shows that greater than 300 milliwatts at 196 nm can be generated from a 10 kHz, 20 watt q-switched Nd:YAG laser. The pulse repetition frequency is 10 kHz.

The q-switched Nd:YAG laser provides 20 watts of average power at 1064 nm. The 1064 nm beam is split into two components: 1.5 watts is diverted to the 196 mixer and 3.5 watts to the frequency tripler. The remaining 15 watts is frequency doubled in a long (> 30 mm) non-critically phase matched LBO crystal. We anticipate greater than 60% conversion efficiency to the green (10.0 watts). The green is also split into two components, 3 watts is used for the 355 nm tripler, and the remaining 7 watts is used to pump the optical parametric oscillator sub-system. These are preliminary calculations and likely the powers at the various stages will change. We also anticipate some downstream optical material issues with the generation of 300 mW at 196 nm in a small diffraction limited beam, so some scaling back of the power may be necessary to accommodate the 196 nm beam handling optics. This laser design will permit power scaling once the coating and substrate issues are solved.

Frequency Doubler and Tripler

The frequency doubling from 1064 nm to 532 nm is done is an external type I non-critically phase-matched LBO crystal. The LBO crystal is 35 mm long and is operated at 149 degrees C. The 20 watts of infrared power is split such that 15 watts are available to the doubler which provides about 10 watts at 532 nm. The 355 nm beam is generated by using 3.5 watts directly from the 1064 nm laser and 3.0 watts of the green doubled light. The third harmonic generator uses type I LBO as well, although with a moderate walk-off of 17 milliradians.

OPO designs

Our team has a great deal of experience with optical parametric oscillator technology, especially in the area of injection seeding to achieve single frequency operation. This is the heart of this system and we are considering several design approaches for the Phase II effort. One conventional method to achieve a single frequency OPO is to use an external cavity diode laser as a seed source at the OPO signal wavelength, in our case 744.7 nm. There are commercially available single frequency diode laser that operate at this wavelength. For example the Sacher Laser Model TEC-500-0740-10 emits 10 milliwatts at 744 nm and has a typical linewidth of less than 300 kHz. One seeded OPO configuration is a travelling wave three mirror ring cavity with the seeder entering the cavity through the output coupler as shown in the schematic in Figure 16. The gain medium is either bismuth triborate (BiBO) or periodically poled lithium tantalate (PPLT). The estimate is that 2 watts of pump power at 532 nm will provide 300 mW of signal output at 744 nm (15% efficiency).

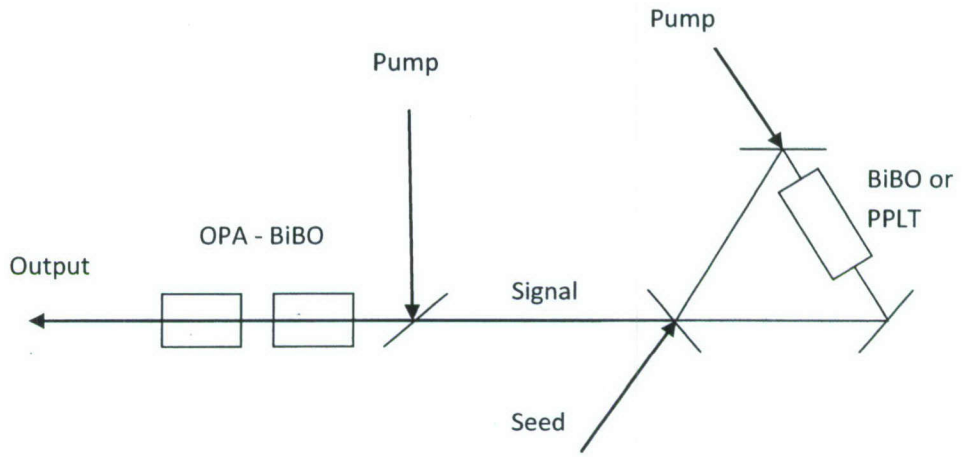

Figure 16: Schematic of an injection seeded OPO in a simple three mirror ring cavity; pump beam enters through mirror that has a high reflectivity for the signal wave and is highly transmitting for the pump. Seed laser enters through output coupler. The OPO signal is amplified by an OPA consisting of two 15 mm long BiBO crystals.

These injection seeded line narrowed OPO schemes can be actively locked by a variation of the build-up time reduction method used in the Nd;YAG laser. In this case the time delay of the OPO signal output pulse as referenced from the Nd:YAG q-switch sync pulse is monitored and kept at a minimum value by dithering the cavity length of the OPO.

To achieve higher power it is standard procedure to construct a MOPA, an optical parametric amplifier (OPA) following the master oscillator, as shown in Figure 16. In this case two 15 mm long type II BiBO crystals are arranged in series. The walk-off in BiBO for this interaction is quite low, about 5.5 milliradians. With approximately 5 watts of pump we expect to attain 1 W at 744 nm, as shown in the SNLO signal energy profile given in Figure 17. Our research partners at Sandia have a great deal of experience in this area and have other methods and techniques that will come into play as we get into

the design and construction of the OPO device and it is thus expected that the energies in the different optical modules will vary to some degree.

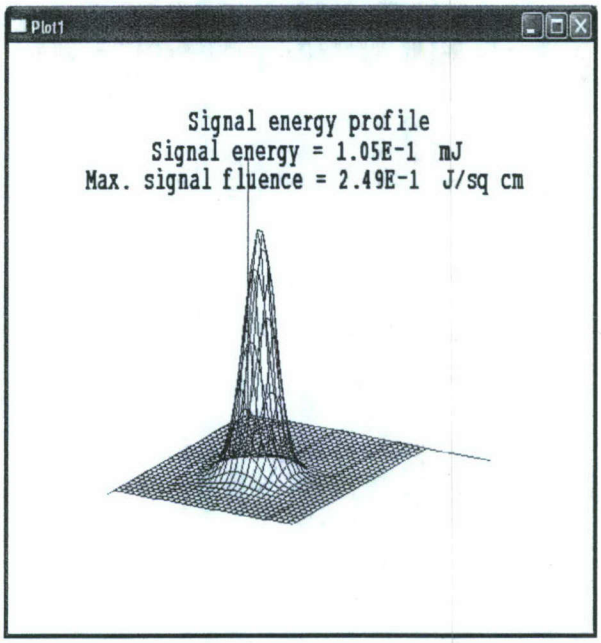

Figure 17: SNLO model of dual crystal (L_c = 15 mm) BiBO OPA; assumes 30 uJ of input pulse energy from the single frequency master oscillator at 744 nm.

We are also exploring a newer technology for line narrowing the OPO – the volume Bragg grating or VBG. The VBG is a block of transparent glass that has a series of closely spaced planes which form a modulation grating of the refractive index. The VBG OPO architecture is advantageous over injection seeding from a number of perspectives: 1) it's less complex - no seed laser is required; 2) it is lower in cost – VBG mirrors cost about $500 versus $20,000 for a diode seeder; 3) high power operating power – a linear cavity VBG OPO in general can provide over one watt of output power, whereas longer ring lasers may require an OPA for higher power.

Actinix used a VBG in the NEMO laser and is currently experimenting with these devices in next generation OPOs. The upper diagram in Figure 18 shows the general concept of our experimental VBG OPO. The pump is the same type of intracavity doubled q-switched laser used in the NEMO system and runs at 7 kHz, with a 15 ns pulse duration. The cavity consists of a short wave pass, one-meter radius of curvature rear mirror that is 85% transmitting to the 532 nm light and 100% reflecting to the 710 nm. The flat VBG mirror has a diffraction efficiency of 75% at 710 nm. The BiBO crystal is 15 mm long and the physical length of the cavity is 43 mm (FSR = 2.7 GHz). The pump beam is focused to a spot size diameter in the BiBO of approximately 220 microns The middle chart in Figure 18 is the modeled bandwidth of the OPO, assuming that the single pass bandwidth of the VBG is 80 pm at 710 nm and that the time the OPO is over threshold is 10 ns, which corresponds to approximately 27 passes on the VBG. The single pass VBG bandwidth divided by the square root of the number of passes determines the bandwidth envelope of the OPO.

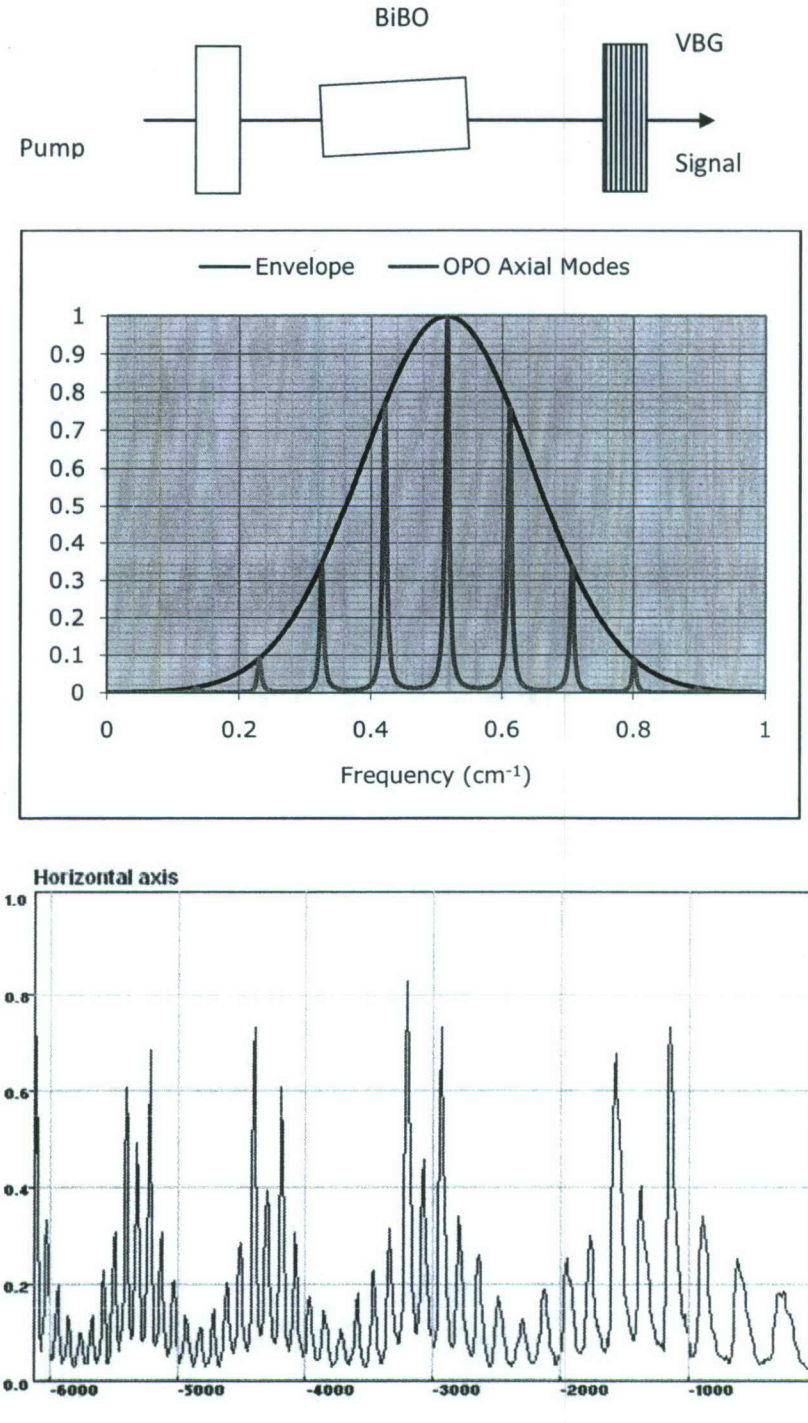

Figure 18*: Upper* - Diagram of experimental 710 nm OPO cavity using a VBG mirror output coupler, a broadband dielectric mirror high reflector and a 15 mm long BiBO crystal. The optical cavity length is 55 mm; ***Middle*** - Modeled axial modes and Gaussian spectral bandwidth assuming the OPO is over threshold for 10 ns; ***Lower*** - Actual spectrum of the experimental VBG OPO analyzed with a 1.0 cm^{-1} FSR Fabry-Perot etalon. The FWHM bandwidth is estimated to be approximately 0.3 cm^{-1}.

The resulting OPO bandwidth at 710 nm is 15.3 pm or 0.3 cm^{-1}. The actual OPO spectrum was measured with a Fabry-Perot analyzer (FSR = 1 cm^{-1}) and verified to be approximately 0.3 cm^{-1} as shown in the lower diagram in Figure 18. The power achieved in this OPO configuration is nearly 1.7 watts power with 7 watts of pump, and a threshold of less than 3 watts (see Figure 19).

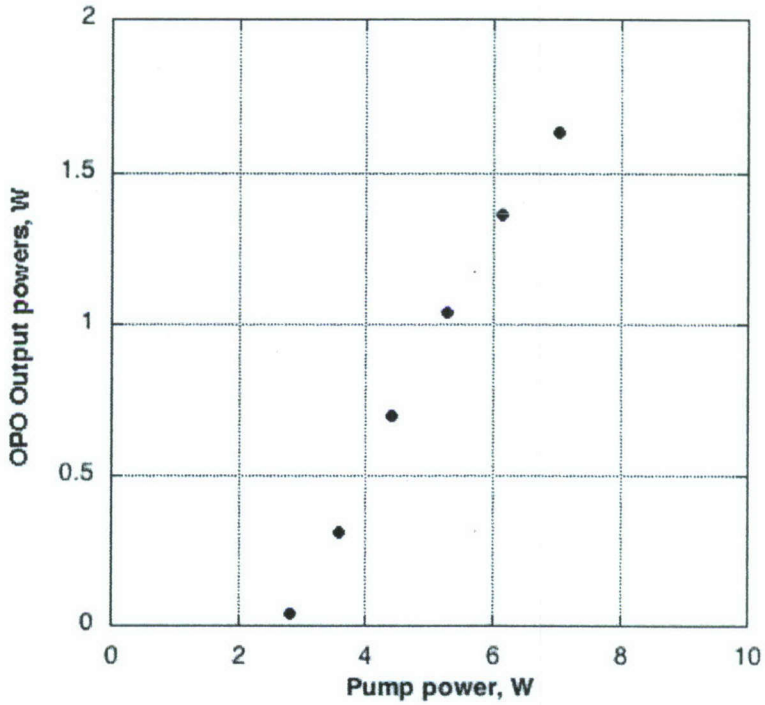

Figure 19: Experimental data of signal output power versus pump power for the narrowband 710 nm VBG OPO shown in the previous figure. The threshold is less than 3 watts and the output power is >1.5 watts with 7 watts pump. This plot shows the viability of this simple linear cavity OPO in providing high output power.

The results shown in Figures 18 and 19 are relevant to building a long coherence light source in that the VBG line narrowing methodology can be taken further by shortening the OPO cavity length and using a second VBG as the back mirror in the OPO cavity. Using a second VBG has the effect of doubling the number of grating passes per cavity round trip. We show this concept for an OPO running at 744 nm in the upper diagram in Figure 20. Here we again use the 15 mm long BiBO crystal but we shorten the physical cavity length to 20 mm, giving us a free spectral range of 4.7 GHz, thus spreading out the axial modes. Our seeded pump laser has a pulse duration of 28 ns versus 15 ns from the previous case, so our assumption is that the oscillation time over threshold increases to 20 ns, implying there are a total 188 passes on the two VBGs. This has the effect of narrowing the envelope of the OPO bandwidth to 3.2 GHz, which is less than the free spectral range of the cavity, thereby permitting single mode oscillation, and we show this modeled in the lower diagram in Figure 20. The issue then is to lock the cavity so it stays on the single axial mode peak. This will be a task for Phase II. We fully expect that between the VBG OPO and the injection seeded OPO we will attain the required linewidth and power performance at 744 nm for the further frequency conversion processes that ultimately generate 196 nm.

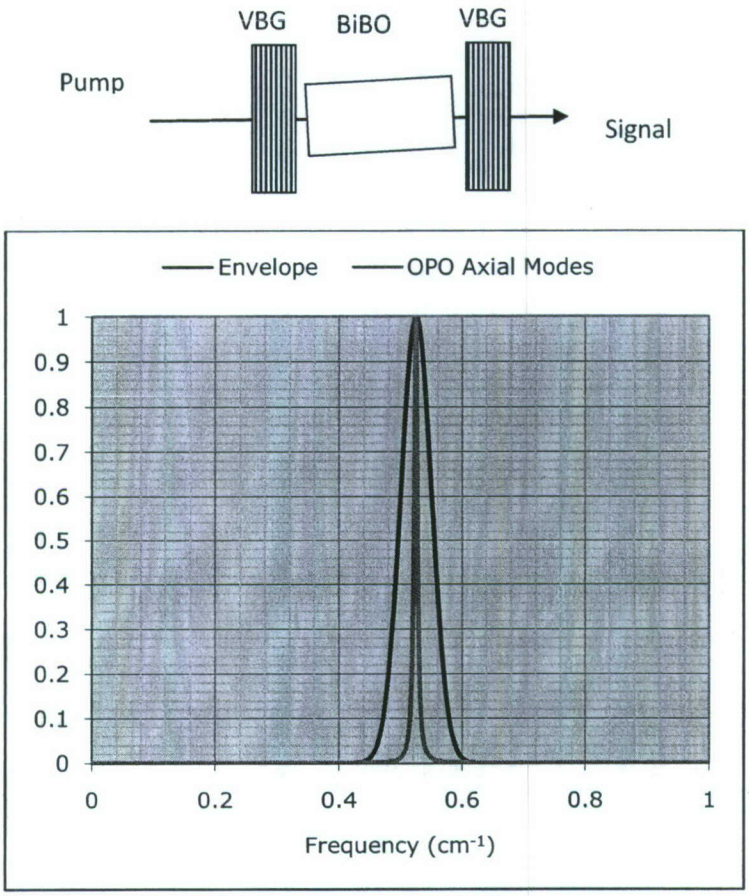

Figure 20: ***Upper*** *– Layout of* OPO with short cavity using two VBGs (high reflector and output coupler) for increased dispersion. ***Lower*** **-** modeled single frequency spectrum

DUV and 196 nm Mixer modules

We gain a significant power advantage in this architecture by virtue of utilizing the 3rd harmonic and fundamental beams of the pump laser as inputs to the DUV and 196 nm mixers. In the DUV mixer we generate 37.5 microjoules (375 milliwatts) at 240.4 nm. This mixer uses a 15 mm long type I CLBO crystal heated to 150 degrees C. The crystal is oriented at 68 degrees and has a moderate walk-off angle of 27 milliradians. The input beam diameters are 250 microns. The SNLO model result is shown in Figure 21.

For the 196 nm mixer we employ a single 15 mm long CLBO crystal operating in the non-critical phase-matching condition at 150 decrees C enabling both high conversion efficiency and excellent spatial mode quality. The 375 milliwatts of 240.4 nm light is mixed with 1.5 watts of the 1064 nm fundamental; both beams are 250 microns in diameter. The SNLO model predicts 250 milliwatts at 196 nm will be generated. It is important to mention here that this high level of pulsed power at 196 nm in a tight, clean spatial mode profile has never been produced before to our knowledge and it likely will be destructive to downstream optical components. We therefore will have to spend design time and resources to build a reliable beam delivery system to handle this high intensity.

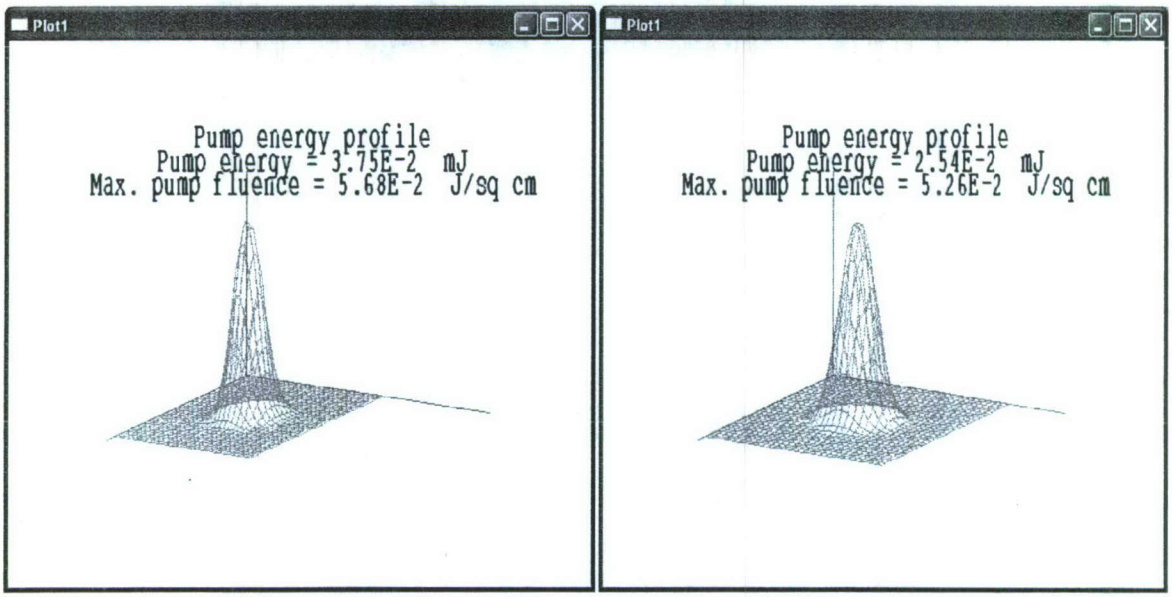

Figure 21: ***Left*** - DUV profile and energy modeled in SNLO; P_{avg} = 375 mW. ***Right*** – 196.1 profile and energy; P_{avg} = 254 mW.

The 240 nm, 196 nm, 355 nm and 532 nm are all heated crystal assemblies and will be packaged in ultraclean, purged housings similar to that shown below in Figure 22.

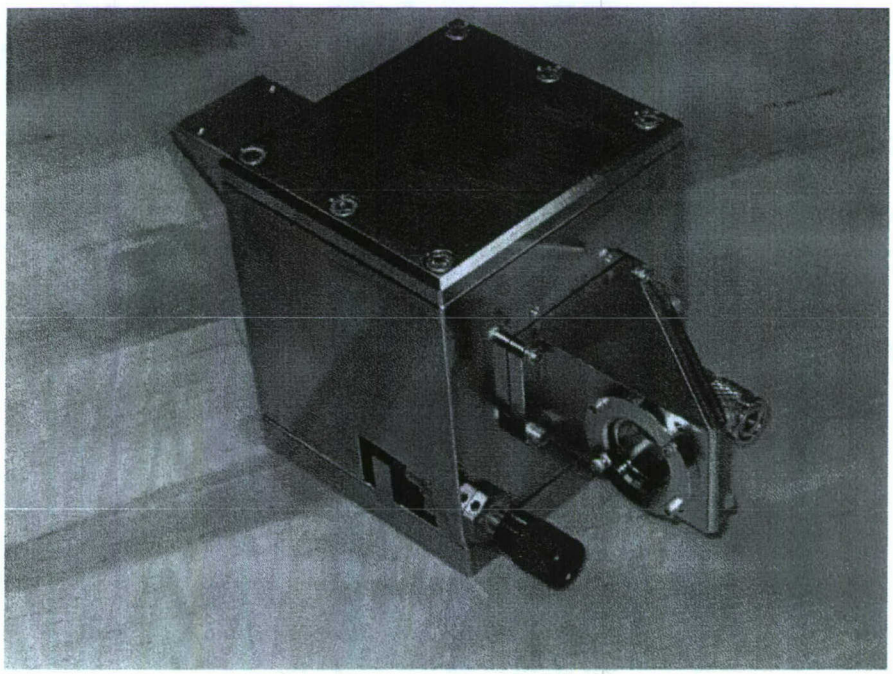

Figure 22. Purged, nickel plated housing containing heaters for either CLBO or LBO crystals. Input/output windows are uncoated and oriented at Brewster's angle.

9. References

A. J. Merriam, J. J. Jacob, D. S. Bethune, and J. A. Hoffnagle, "Efficient nonlinear frequency conversion to 193-nm using cooled BBO", *2007 Advanced solid-state photonics conference proceedings, in press.*

J. A. Hoffnagle et al., "Liquid immersion deep-ultraviolet interferometric lithography", *Journ. Vac. Sci. Tech* B, **17** (6), pg. 3306 -3309 (1999)

A. J. Merriam, D. S. Bethune, J. A. Hoffnagle, M. Jefferson, J. J. Jacob and T.J. Litvin, "A solid-state 193-nm laser with high-spatial coherence for sub-30-nm interferometric immersion lithography", *Proc. SPIE,* **6520**, (2007) *in press.*

R. L. Farrow, D. A. V. Kliner, G. R. Hadley, and A. V. Smith, "Peak-power limits on fiber amplifiers imposed by self-focusing," Opt. Lett. 31, 3423-3425 (2006).

D. A. V. Kliner, F. Di Teodoro, J. P. Koplow, S. W. Moore, and A. V. Smith, "Efficient second, third, fourth, and fifth harmonic generation of a Yb-doped fiber amplifier," Opt. Comm. 210, 393-398 (2002).

G. R. Hadley and A. V. Smith, "Self-focusing in High-Power Optical Fibers," SPIE Photonics West, San Jose, CA (2007), in SPIE Proceedings conf. on fiber lasers IV: technology, systems, and applications, 6475, 64750G-1-11 (2007).

G. R. Hadley, R. L. Farrow, and A. V. Smith, "Three-dimensional time-dependent modeling of high-power fiber amplifiers," SPIE Photonics West, San Jose, CA (2007), in SPIE Proceedings conf. on fiber lasers IV: technology, systems, and applications, 6453, 64531B-1-10 (2007).

R. L. Farrow, G. R. Hadley, A. V. Smith, and D. A.V. Kliner, "Numerical modeling of self-focusing beams in fiber amplifiers," SPIE Photonics West, San Jose, CA (2007), in SPIE Proceedings conf. on fiber lasers IV: technology, systems, and applications, 6453, 645309-1-9 (2007).

G. R. Hadley, R. L. Farrow, and A. V. Smith, "Bent-waveguide modeling of large-mode-area, double-clad fibers for high-power lasers," SPIE Photonics West, San Jose, CA (2006), in SPIE Proceedings conf. on Fiber lasers III: technology, systems, and applications, 6102, 61021S-1-7 (2006).

S. J. Brosnan and R.L. Byer, "Optical Parametric Oscillator Threshold and Linewidth Studies", IEEE Journal of Quantum Electronics, QE-15, 415-432 (1979).

10. Budget

Sandia National Labs

Dr. Arlee Smith, Research Scientist

Total time on project: 22 days

Total SNL costs: $32,677

Actinix

James Jacob, Principal investigator

Total time on project: 538 hours

Direct labor cost: $33,721

Andrew Merriam, senior personnel

Total time on project: 80 hours

Direct labor cost: $4173

Overhead (@ 75% direct labor costs): $28,420

Total Actinix: $66,314

Total contract costs: $98,991

Acknowledgements – We would like to thank DARPA for supporting this STTR project on this important technology for the mission of MTO and for our continued business development in the U.S. semiconductor infrastructure. We also wish to thank Sandia National Labs for their support in the transfer of technology for this effort.

Chapter 1

Introduction

The goal of this project is to generate 193-195 nm light with a linewidth less than 3 GHz over a time of several seconds. The average power should be 100 mW or more. A fiber based system is preferred, with short, powerful pulses enabling wavelength conversion in a single pass through the nonlinear crystals, rather than CW operation that would require build up cavities around the crystals.

The architecture of the system is constrained by the crystals available for the final mixing stage. A CLBO final stage is attractive because it can noncritically phase match 234.5 nm + 1103 nm → 193.4 nm at a crystal temperature of 410K. An LBO final stage in place of CLBO is unpromising because phase matching requires that the red wave be longer than 2500 nm so it would be strongly absorbed by LBO. Another crystal that can transmit to 193 nm is CBO which can be critically phase matched using 1303 nm + 227 nm but d_{eff} approaches zero as noncritical phase matching condition is approached. KBBF can also transmit but it cannot phase match noncritically. Besides, it is difficult to obtain samples. LB4 can noncritically phase match 1226.6 nm + 229.6 nm → 193.4 nm but $d_{\text{eff}} = 0.18$ pm/V, much smaller than CLBO. The conclusion is that CLBO is the only reasonable choice for the final mixing stage.

A fiber based system might be developed on the 938 nm, Nd-doped silica fiber laser demonstrated by Dawson *et al.*[DDB+06]. The 938 nm light would be frequency quadrupled to 234.5 nm, then summed in CLBO with 1103 nm light from a Yb^{3+} doped fiber amplifier to produce the 193.4 nm light. However, the demonstrated 938 nm fiber operates either cw or quasi cw producing 2 μs pulses, and this does not provide the needed short, powerful pulses. Questions about this laser that must be addressed include: Can pulses a few nanoseconds long be amplified in the fiber without sacrificing efficiency? What linewidth can be expected from a fiber amplifier seeded by 1-5 ns pulses, considering Kerr self phase modulation and perhaps Kramers-Kronig self phase modulation as well? What conversion efficiency to 193.4 nm is realistic? What is the best pulse repetition rate for the lasers? Will an 1103 nm Yb^{3+}-doped fiber amplifier work both cw for a seed and pulsed for the amplifier? Are there likely to be thermal issues with the nonlinear crystals at the power levels required? Should I develop a numerical model for the 938 nm fiber amplifier?

An alternative fiber based, pulse system would use 1080 nm fiber amplifiers. This is better developed technology that the 938 nm fiber, but getting sufficient power to make 100 mW at 193 nm from the 1080 nm fiber is a question that must be answered. Self phase modulation will limit the pulse energy. Efficiency of the system is another potential problem, as is scalability in power.

A third system would use a 946 nm laser as the primary drive. This would be quadrubpled and summed with 1080 nm light to make the desired 194 nm. Such a system could be pulsed for easiest nonlinear conversion, or it could be CW for better efficiency and power scalability. A CW system

would require enhancement cavities for each of three mixing stages. However, the cavity designs could be similar to minimize complexity.

We study each of these three systems in the following three chapters.

Chapter 2

938 nm + 1103 nm system

In this chapter we assess a system based on the 938 nm fiber laser. We assume pulse durations of a few nanoseconds from the fiber amplifier so SBS is minimized, yet peak power is high enough to convert efficiently. We will look at two pulses that bracket the reasonable operating range, a 20 ns, 100 μJ pulse and a 1 ns, 0.5 μJ pulse. The final choice might be somewhere between them, but these two illustrate the trade offs required.

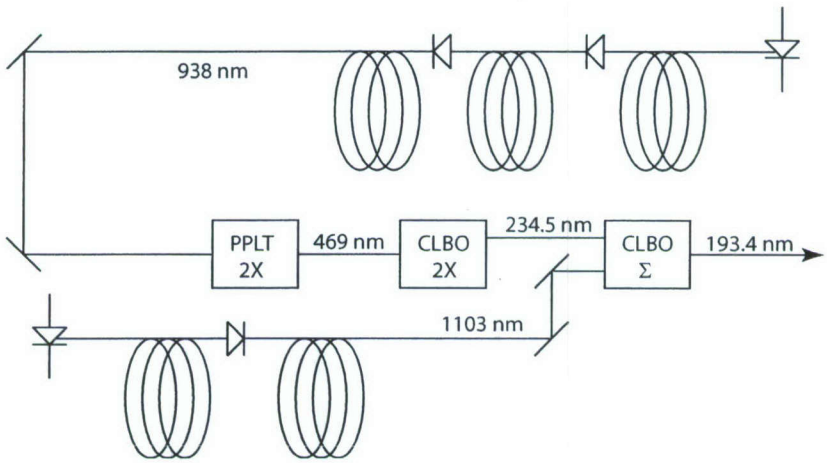

Figure 2.1: Method for producing pulsed 193.4 nm light. The exact wavelengths may differ slightly.

2.1 cw 938 nm fiber amplifier

The cw version specs are listed here[DDB+06]. The output power of stage one was 0.875 W and the output power of stage two was 15 W.

cw 938 nm stage one fiber

length	pump power	pump wavelength	core diameter	core NA	cladding diameter	gain	coil diameter	power out
25 m	35 W	808 nm	20 μm	0.06	125 μm	10 dB	80 mm	3.5 W

cw 938 nm stage two fiber

length	pump power	pump wavelength	core diameter	core NA	cladding diameter	gain	coil diameter
40 m	90 W	808 nm	30 μm	0.06	125 μm	8 dB	80 mm

2.2 Pulsed 938 nm fiber amplifier

pulsed 938 nm stage two fiber

prf	pulse duration	pump power	pump wavelength	core diameter	core NA	cladding diameter	power out	coil diameter
100 kHz	2 μs	90 W	808 nm	30 μm	0.06	125 μm	10 W	80 mm

2.3 Mode profiles

The third order nonlinear processes such as self phase modulation (SPM), stimulated Brillouin scattering (SBS), and stimulated Raman scattering (SRS) depend on the effective mode area of light in the fiber, so we compute A_{eff} here. Fig. 2.2 shows the lowest order mode of the first and second coiled amplifier fibers. A_{eff} is the effective modal area defined by

$$A_{\text{eff}} = \frac{\left[\int u_i^2(x,y)dxdy\right]^2}{\int u_i^4(x,y)dxdy} \tag{2.1}$$

where $u_i(x,y)$ is the normalized transverse mode profile of the ith mode. The effective areas for the stage one and stage two fibers are 238 and 375 μm^2.

2.4 SPM linewidth broadening

The linewidth requirement for the 938 nm light is that it be less than 1 GHz. The primary source of linewidth broadening in the fiber amplifier is self phase modulation. Self phase modulation has contributions from the nonlinear refractive index, n_2, and from a Kramers-Kronig phase related to

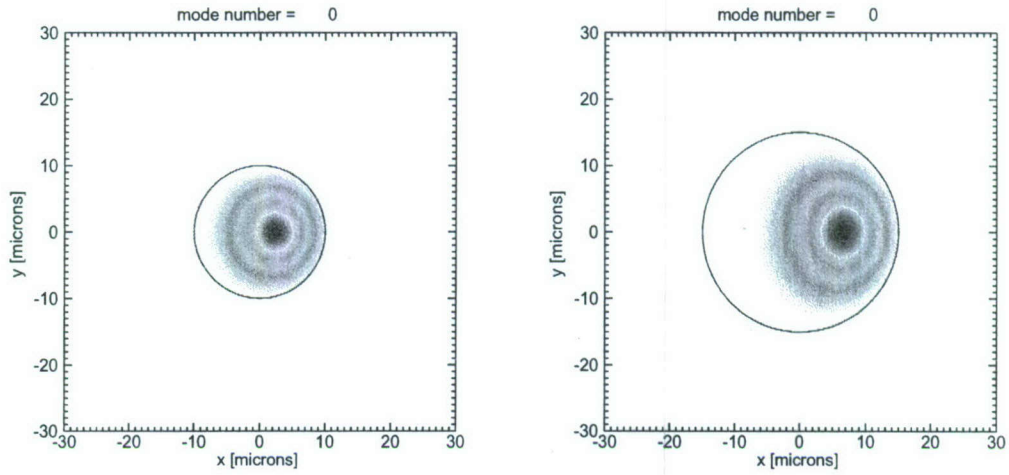

Figure 2.2: The profile of the lowest transverse mode of the first amplifier fiber (left) and the second amplifier fiber (right) of Dawson *et al.*[DDB+06]. The modes are distorted by the fiber bend and have effective mode areas $A_{\text{eff}} = 238$ (left) and 375 (right) μm^2.

the changes in population inversion and refractive index as the pulse passes by. Usually the n_2 contribution is the larger of the two, and better characterized. I do not include a Kramers-Kronig contribution in the calculations presented below.

The equation governing SPM by n_2 is

$$\frac{\partial A(t)}{\partial z} = i\frac{\omega n_2}{cA_{\text{eff}}}|A(t)|^2 A(t) - \frac{\alpha}{2}A(t) \tag{2.2}$$

where $A(t)$ is the square root of the optical power. For silica, $n_2 = 2.66 \times 10^{-20}$ m^2/W.

The SPM linewidth depends on the pulse duration, with shorter pulses giving greater spectral broadening for a fixed pulse energy. I first model SPM in the second fiber amplifier of Dawson using the properties listed in the table above labeled pulsed 938 nm stage two fiber. The pulse is assumed Gaussian in time. The other properties are the same as the cw stage two fiber listed in the table labeled cw 938 nm stage two fiber. I vary the pulse duration, keeping the pulse repetition frequency at the 10^5 pulses per second used by Dawson, and keeping the output pulse energy fixed at 100 μJ. The optical gain in stage two is set to 10 dB. For a 20 ns pulse the broadening is approximately 1 GHz as shown in Fig. 2.3. Shorter pulses of this energy broaden beyond the 1 GHz requirement. The Raman gain exponent for this pulse is 19.6, which is slightly above the SRS threshold. Usually a gain exponent of 16 is considered the SRS threshold, but this might be on the low side.

My conclusion is that if 100 μJ pulses are used they must have a duration longer than 20 ns, so the peak power would be 5 kW. If the gain in the two fiber amplifier stages is 20 dB, the input pulse energy must be 1 μJ. This is probably too much to be supplied by a diode laser.

Shorter pulses with lower pulse energy and higher repetition rate might be a better choice. If we want to use 1 ns pulses, the energy must be less than 0.5 μJ to keep the SPM spectral broadening below 1 GHz. The peak power would be 500 W, which reduces the Raman gain far below threshold.

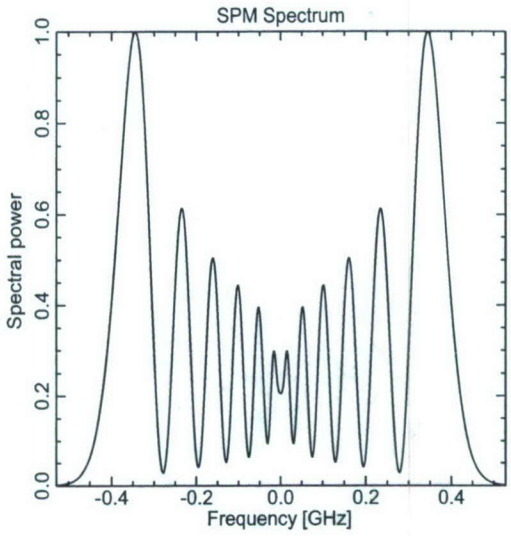

Figure 2.3: The spectrum of a 20 ns, 100 μJ pulse from the second fiber stage.

The required seed pulse energy would be 5 nJ. This would give the spectrum of Fig. 2.4. Achieving 10 W output power at 938 nm implies a pulse repetition rate of 2×10^7 pps.

2.5 1103 nm fiber laser

Koheras offers Bragg grating stabilized fiber lasers in this wavelength range, I think. Making the required 1 ns pulses for amplification in a Yb^{3+}-doped fiber should not be a problem. This will use a short fiber, perhaps 1-3 m long, and pulse energy will be in the μJ range so SPM, SRS, and SBS should be negligible.

2.6 Stimulated Brillouin scattering

Defeating SBS in the second stage 938 nm fiber is a major issue. The approximate SBS gain equation for a long pulse is[Agr89]

$$\frac{\partial A_S}{\partial z} = -\frac{g}{2A_{\text{eff}}}|A_L|^2 A_S \tag{2.3}$$

and the SBS threshold corresponds to

$$\frac{gL_{\text{eff}}}{2A_{\text{eff}}}|A_L|^2 = 20 \tag{2.4}$$

making the laser power SBS threshold

$$|A_L|^2 = \frac{40A_{\text{eff}}}{gL_{\text{eff}}}. \tag{2.5}$$

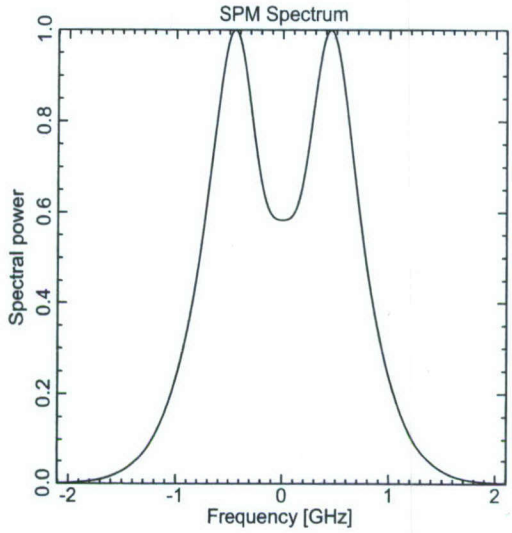

Figure 2.4: The spectrum of a 1 ns, 0.5 μJ pulse from the second fiber stage.

The gain coefficient for SBS is $g = 5 \times 10^{-11}$ m/W, the Stokes shift is 18 GHz, and the acoustic wave decay time is approximately 5 ns at 18 GHz. For the 20 ns, 100 μJ pulse, the effective gain coefficient is 5×10^{-11} m/W, the peak power is 5 kW, and the effective length is 4 m, giving a threshold of approximately 75 W for an unchirped pulse. The SPM-induced chirp reduces L_{eff} to approximately 0.3 m which raises the SBS threshold to 1 kW, still below the 5 kW peak power of the pulse, so the 20 ns, 100 μJ pulse will probably suffer from SBS. For the 1 ns pulse L_{eff} stays at 0.3 m, but g is reduced because the pulse is shorter than the acoustic damping time, so the threshold power will increase somewhat. I conclude that a 20 ns, 100 μJ pulse is above the SBS threshold, but a 1 ns, 0.5 μJ pulse is not. The 1 ns pulse seems safe from nonlinear problems, so the next step is to see whether it can be converted to 193.4 nm with sufficient efficiency to meet the system requirements.

2.7 First SHG stage 938 nm $\rightarrow$ 469 nm

I chose QPM $LiTaO_3$ (PPLT) as the first stage doubling crystal. Its d_{eff} is 9 pm/V, and the required poling period is 5.2 μm. Literature reports indicate 300 μm thick PPLT has been poled with 2.3 μm period[CPTM00]. Furthermore, 7 W at 530 nm has been generated in a 15 mm PPLT[GPT04] crystal, and 7 W at 542 has been generated in a 20 mm crystal[TKK07]. Lengths up to 40 mm and periods down to 1.3 μm have been demonstrated[MLK$^+$01]. Periods as short as 8 μm have been created in 1 mm thick crystals[YKNK04].

According to the model run illustrated in Fig. 2.5, 20 mm of PPLT can give greater than 80% conversion of a 1 ns, 0.5 μJ 938 nm pulse to 469 nm. Starting with 10 W at 938 nm we get 8 W at 469 nm.

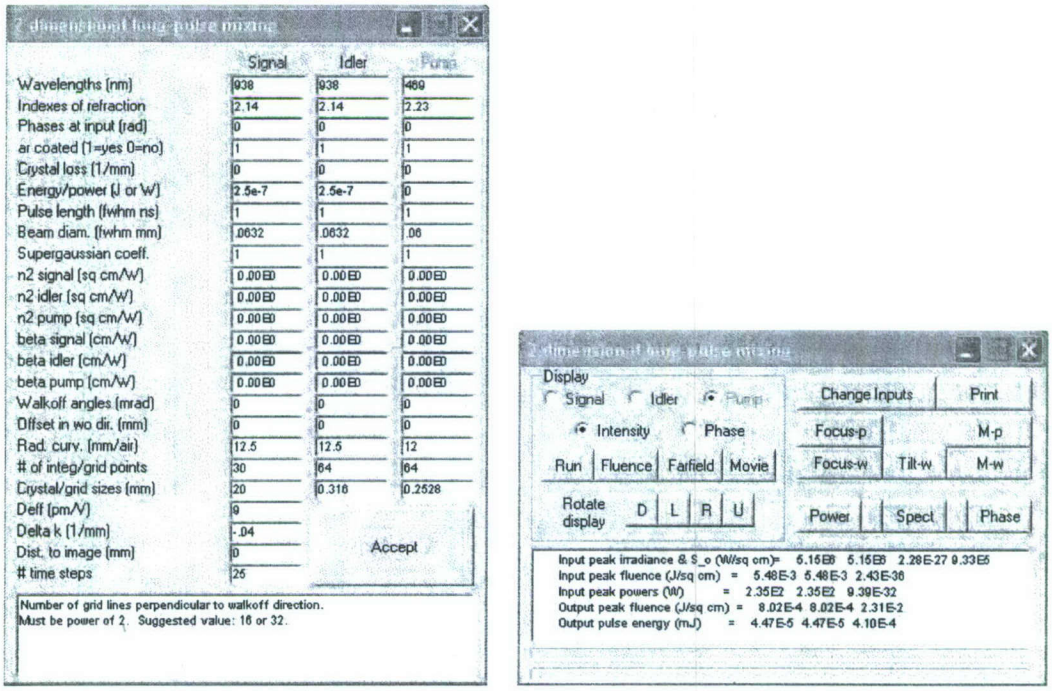

Figure 2.5: Model of doubling 938 nm light in PPLT.

2.8 Frequency doubling stage two

How to double the 469 nm pulses to 234.5 nm? Is BBO the best choice? What efficiency can be achieved? Heating is always a concern with BBO. The best way to avoid thermal problems usually is to use a longer crystal with larger beams, but the large walk off in BBO makes long crystals problematic. One solution is to use walk off compensating crystals. Using a single 20 mm long crystal gives a doubling efficiency of approximately 5% and generates a highly elongated second harmonic beam. Switching to ten walk off compensating, 1 mm long crystal segments gives a nearly round beam and 20% conversion efficiency. The mixing conditions for the walk off compensated doubler are listed in Fig. 3.4, and the second harmonic beam profile is shown in Fig. 2.7. Of course using 10 crystals is possible only if they have really good anti reflection coatings for both the fundamental and second harmonic. The phase shifts in these coatings are a big deal as is properly orienting the crystals. One advantage of segmenting the crystals might be better cooling by sending a smooth flow of air over the crystal faces. If we can achieve even 10% efficiency the 234.5 nm power would be 800 mW, still in the game for a 100 mW source.

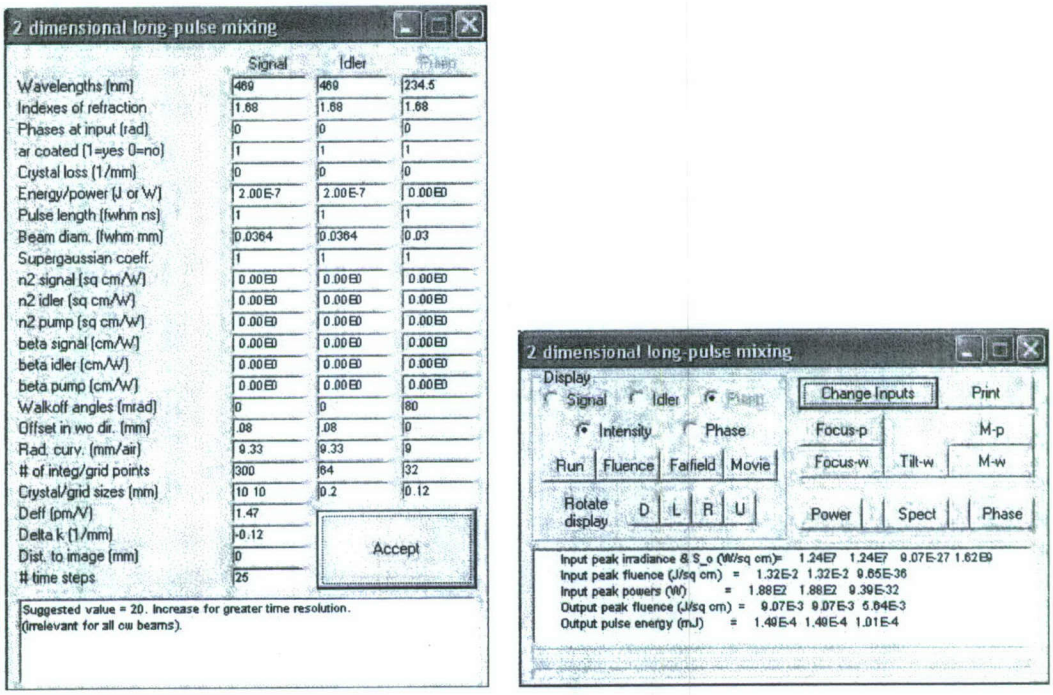

Figure 2.6: Model of doubling 469 nm light in BBO.

2.9 Sum frequency mixing

It appears that CLBO is the only choice for this stage. At T=430K this is angle noncritical with $d_{\text{eff}} = 1.11$ pm/V. What 1103 nm power is needed to convert the 400 mW of 234.5 nm light to 100 mW at 193 nm? Using a 20 mm long CLBO crystal with 50 nJ, 1 ns pulses of 1103 nm light summed

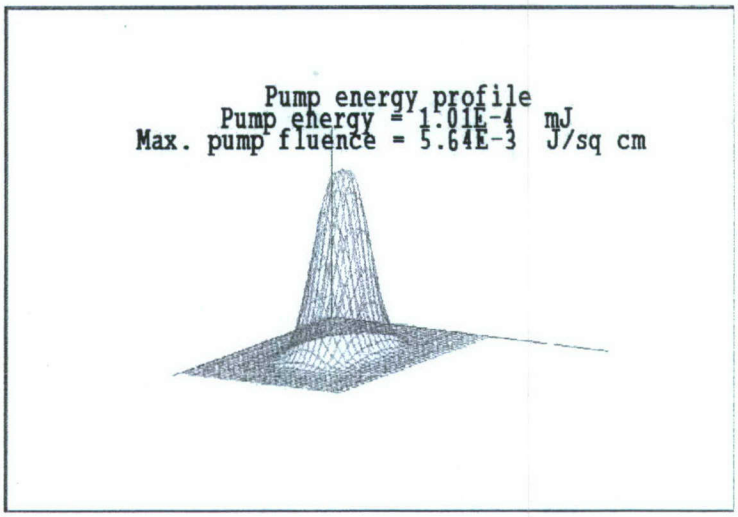

Figure 2.7: Profile of the 234.5 nm beam using 10 walk off compensating, 1 mm long BBO crystals.

with the 400 mW of 234.5 nm light gives an output power of over 500 mW. This is using 10% as the stage two conversion. The inputs and output of this model are shown in Fig. 2.8.

2.10 Pulse duration scaling

Everyone knows the ideal mixing conditions above cannot be fully realized, but the goal of 100 mW seems within reach of this design. If 3 ns pulses are used in place of 1 ns pulses, the pulse energy can be increased by 9 without additional SPM broadening, which will increase the peak power by 3. This should increase the conversion efficiency, but the pulse repetition rate would be reduced by 9, so it is not obvious how much higher the output power would be. More modeling is needed to assess this.

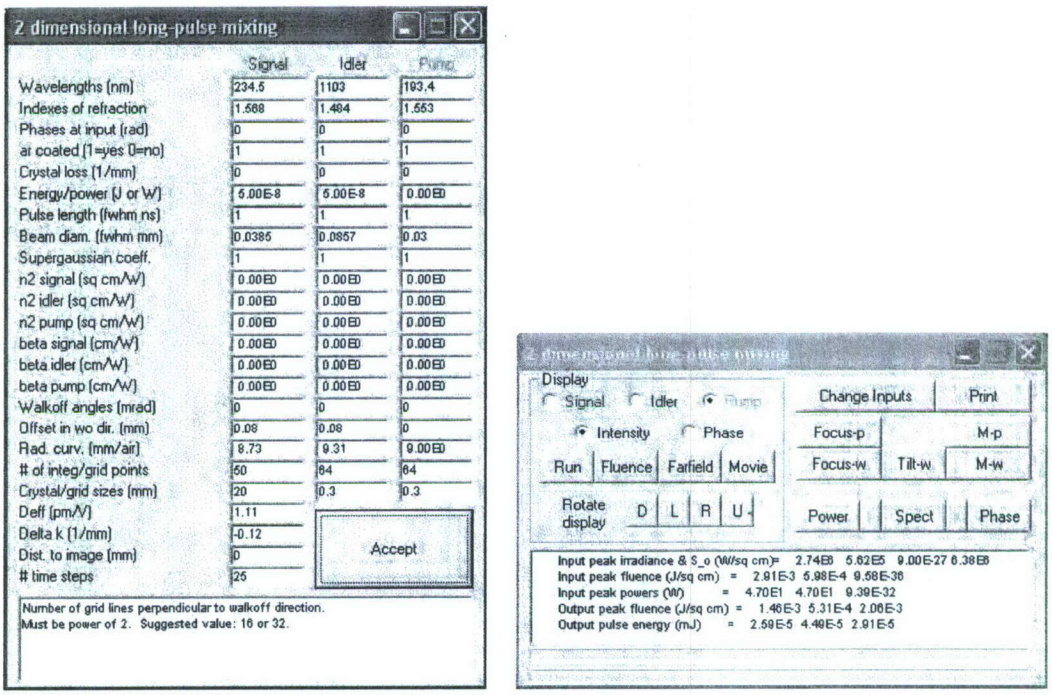

Figure 2.8: Model of sum frequency mixing 234.5 and 1103 nm light to generate 193.4 nm light in 20 mm CLBO crystal.

Chapter 3

Pulsed 1080 nm fiber based design for generating 195 nm light

This design produces 195 nm light rather than 193.4 nm light. This allows mixing in the final stage with wavelengths longer than 1073 nm rather than longer than 1095 nm, the requirement when generating 193.4 nm light. The shorter wavelength makes it possible to use Yb^{3+} doped fiber closer to its gain maximum. Such fiber lasers operate most efficiently in the range 1030 - 1080 nm.

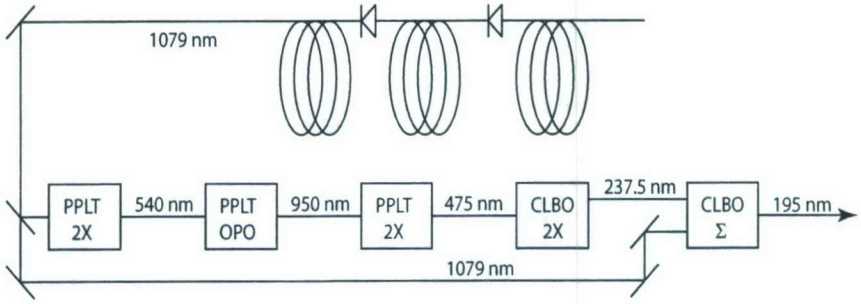

Figure 3.1: Method for producing pulsed 195 nm light. The exact wavelengths may differ slightly.

The final two crystals in this scheme are identical. CLBO can noncritically phase SHG of 475 nm light at T=376 K with $d_{\text{eff}} = 0.94$ pm/V. At the same temperature, the wavelength combination 1079 nm + 237.5 nm also noncritically phase matches for 194.7 nm generation in CLBO with $d_{\text{eff}} = 1.1$ pm/V. The source of 475 nm light could be the frequency doubled output from a 950 nm OPO, pumped by the frequency doubled 1079 nm pulses at 539.5 nm. If we choose a repetition rate of 10 kHz the output pulse energy required for an average power of 100 mW is 10 μJ. We use this to work backward through the system to find the required pulse energy from the 1079 nm fiber laser.

3.1 Final stage 238 nm + 1079 nm → 195 nm

In a 10 mm long crystal complete upconversion of a weak 238 nm beam requires 10^7 W/cm^2 at 1079 nm. This is a fluence of 0.01 J/cm^2 which should be well below the damage threshold of the crystal. The 237.5 nm pulse will be shorter than the 1079 nm pulse so we can consider the 1079 nm

light almost constant over the mixing time. We can also make the 1079 nm beam larger in diameter than the 237.5 nm beam to best approximate the required 10^7 W/cm2. Nearly 100% conversion is possible using the conditions shown below. This requires approximately 150 μJ pulses, or 1.5 W of 1079 nm light at 10 kHz repetition rate to the final mixing stage.

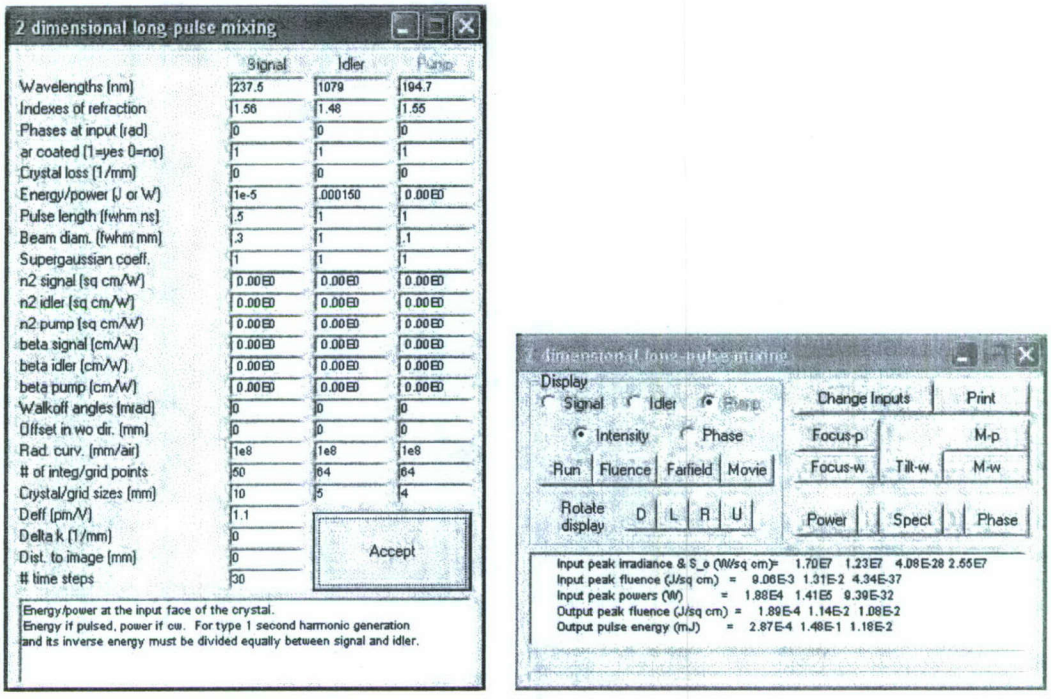

Figure 3.2: Modeling (238 nm + 1079 nm → 195 nm) in a 10 mm CLBO crystal.

3.2 Second SHG stage 475 nm → 238 nm

We next consider the CLBO doubler that converts 475 nm pulses to 237.5 nm. The input pulse duration is assumed to be 0.5 ns. We need to generate 10 μJ output at 237.5 nm. This can be done in a 10 mm CLBO crystal with 15 μJ of 475 nm light in a half nanosecond pulse, as shown in Figure 3.3. With 14 μJ of 475 nm light we predict 10 μJ at 238 nm.

3.3 First SHG stage 950 nm → 475 nm

So far, so good. We move on to the generation of the 475 nm light by frequency doubling 950 nm pulses. The preferred method is doubling 950 nm light. The average output power is 10 kHz × 15 μJ or 150 mW. This low average power makes it possible to use a periodically poled crystal, such as PPKTP, PPLNB, or PPLT. PPLT is probably the best choice for blue light generation. It can generate 150 mW of blue light without damage[HLL+02, HHZ+03, HZZ+07]. The poling period is 5.5 μm, and this is available commercially from Raicol Crystals, HC Photonics, Spectralus, and

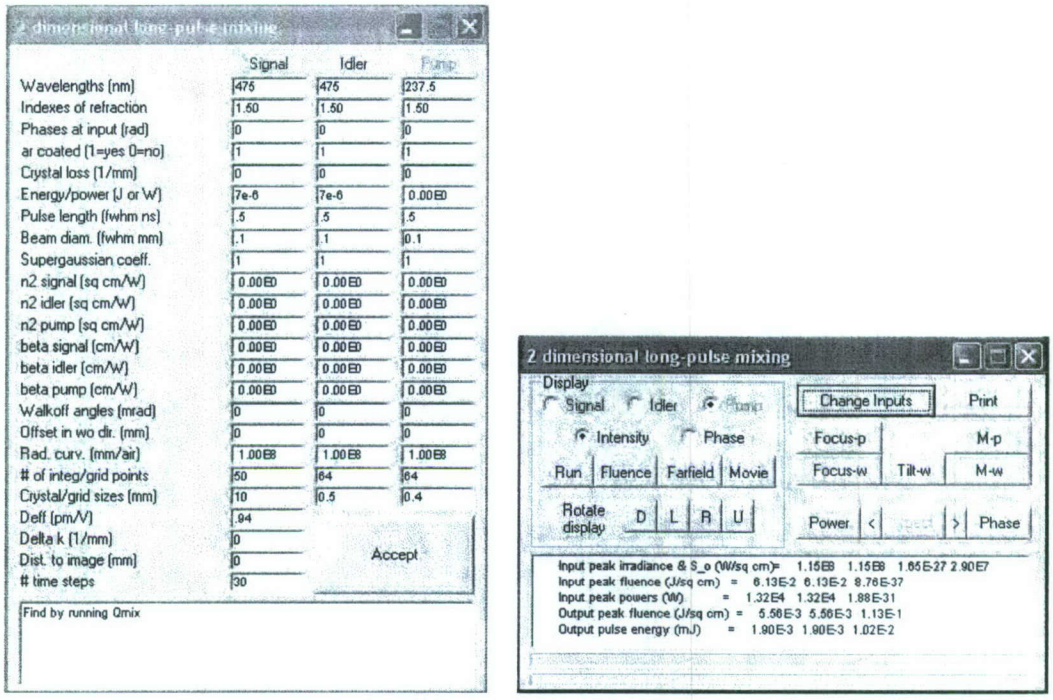

Figure 3.3: Modeling (475 nm $\rightarrow$ 238 nm) in a 10 mm CLBO crystal.

Oxide Corp. The model predicts that an input energy of 20 μJ in a 0.5 ns pulse with a 10 mm long crystal PPLT can give the desired 15 μJ output. The irradiance levels required appear to be well below those that cause blue-light-induced infrared absorption[HPWL07]. This model is shown in Figure 3.4.

3.4 Pulsed fiber amplifier at 1080 nm

A Yb^{3+} doped fiber has gain at 1080 nm. We need to generate at least 150 μJ at 10 kHz repetition rate. We model the performance of a commercially available, large mode area, polarization maintaining fiber[SFF+08]. It has a core diameter of 50 μm, a cladding diameter of 250 μm, and a length of 0.8 m. Using 10 W of 976 nm diode pumping the output end of the fiber, and seeding with 1 ns, 5 μJ pulses gives 150 μJ output pulses with the spectrum shown in Figure 3.5. The spectral width of nearly 2 GHz is a large fraction of the 195 nm budget of 3 GHz. A smaller core fiber would be more efficient but would give a broader spectrum. The modeled case is not necessarily the optimum design, but it is not far off.

We showed above only the final fiber amplifier stage taking the energy from 5 μJ to 150 μJ. If we start from a cw fiber laser we must amplify from 200 mW cw to pulses of 5 μJ. This is a gain of 2.5×10^4 which would probably require two and maybe three stages with isolation and ASE removal between stages. This is getting complicated and expensive. Nevertheless, there is one more stage to evaluate and that is the 950 nm source, which might be an OPO pumped by 100 μJ, 1 ns long pulses at 540 nm, obtained by frequency doubling a 1080 nm pulse.

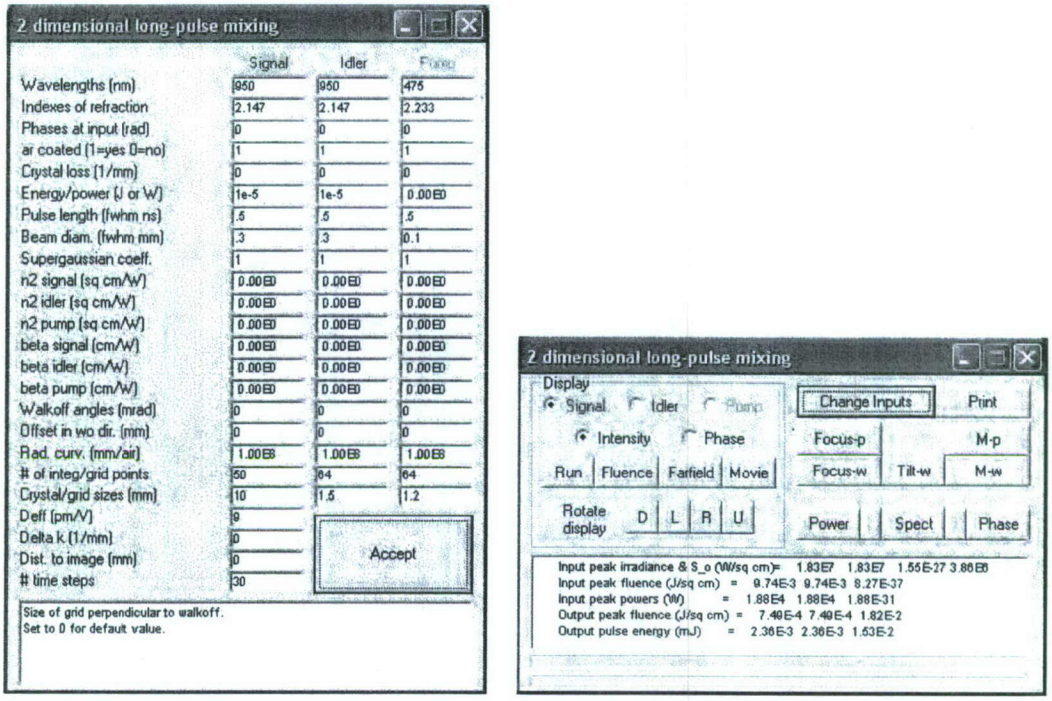

Figure 3.4: Model of frequency doubling 950 nm pulse to 475 nm in 10 mm PPLT crystal. The input beam diameter is 300 μm and the pulse duration is 0.5 ns.

3.5 950 nm OPO pumped by 540 nm pulses

Can 100 μJ, 1 ns pulses at 540 nm make an OPO oscillate to generate 20 μJ, 0.5 ns pulses? Yes, and Figure 3.6 shows one example. It may not be optimum, but it demonstrates feasibility using a 3 mm long PPLT in a 10 mm long standing wave, singly resonant, single pass pumped OPO. The 540 nm pump light is generated by doubling the output of a 1080 nm fiber amplifier similar to that described in the previous section.

3.6 Conclusions on 1080 nm fiber pumped system

Pulsed fiber lasers are not ideally suited to this application because it is difficult to saturate their gain over a sufficient length of fiber to obtain the needed pulse energy without also spectrally broadening the pulse beyond the required 0.1 cm^{-1}. On the other hand, cw fibers can be extremely efficient and can provide high power, making a cw 195 nm source feasible. We look at that below. If we stick with a pulsed system, a design based on a 946 nm pulsed laser has some attractive features. We can study this as well if desired.

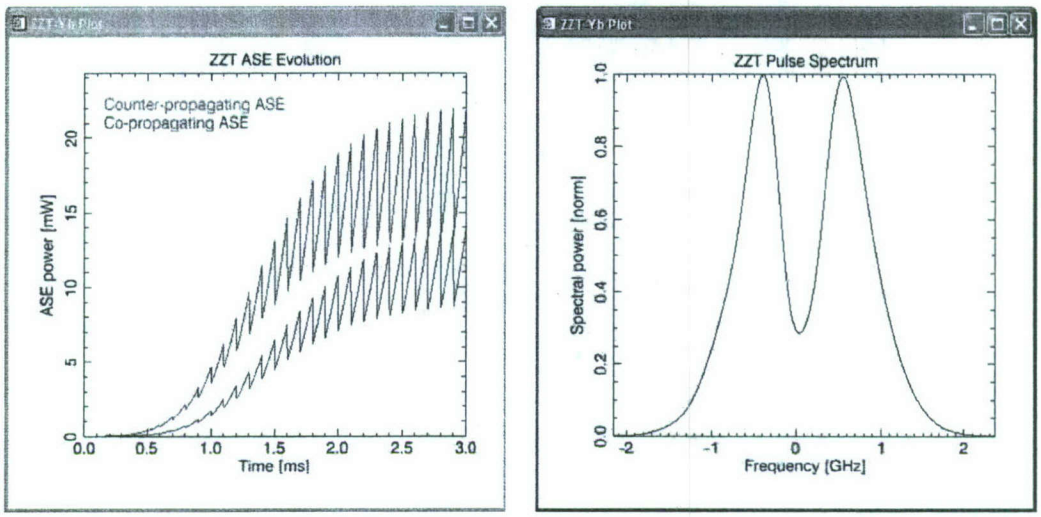

Figure 3.5: Model of 1080 nm pulse amplification in a large mode area fiber. The ASE plot shows the turn on transient for the amplifier, and the modulation shows the gain depletion from the nanosecond pulse amplification. The pulse spectrum is broadened by self phase modulation.

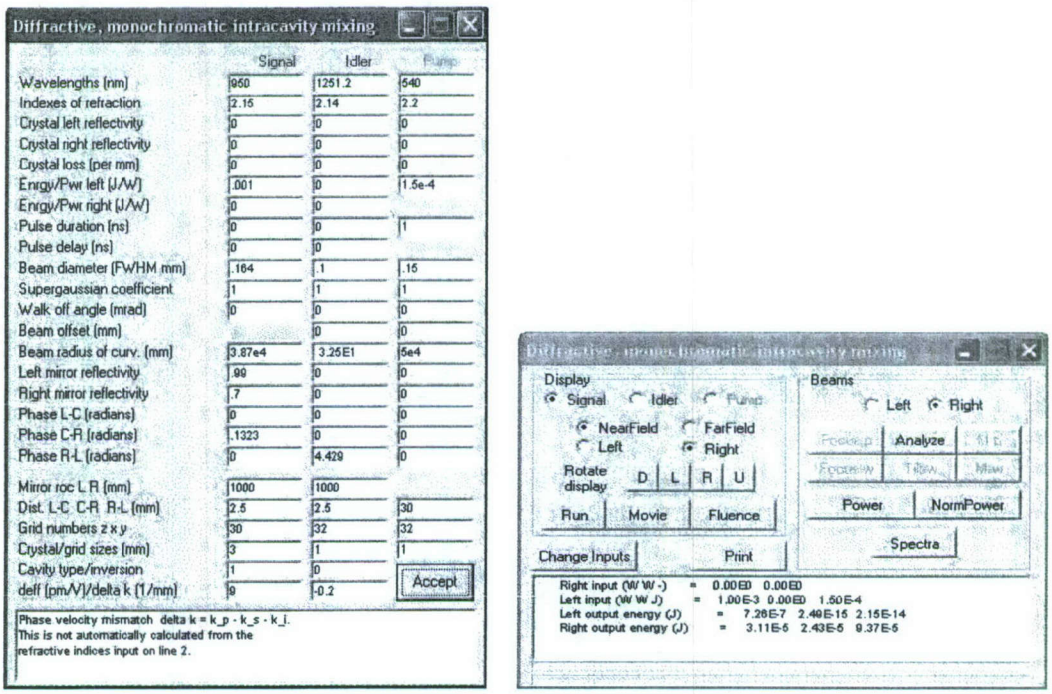

Figure 3.6: Model of OPO for generation of 20 μJ of 950 nm light starting with 150 μJ of 540 nm light.

Chapter 5

CW 1080 nm fiber laser based system

This scheme is the same as the pulsed 1080 nm pulsed fiber scheme of Chapter 3 except all the lasers are CW. The challenge is attaining the required 100 mW starting from roughly 10 W at 1080 nm. The scheme is shown in in Figure 5.1. It is built around noncritically phase matched CLBO crystals for the final two stages and PPLT for the first three stages. All of the stages probably require build up cavities to achieve adequate mixing efficiency.

In the discussions below I use characteristic powers, called $\mathcal{P}_\circ$ which differ for each mixing process. These can be calculated using the 2D-mix-LP model under conditions of weak mixing using the formulas given in the discussion. From these characteristic powers the efficiencies of each stage can be approximated using the given analytic expressions. In each case I have verified these efficiencies using the 2D-cav-LP models. These models typically take many minutes to run so the analytical expressions can be used to quickly try variations on the mixing parameters; you just need to find $\mathcal{P}_\circ$ for each and use it in the formulas.

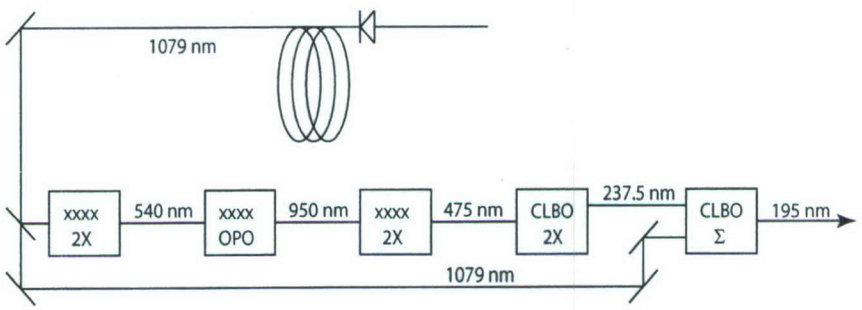

Figure 5.1: Method for producing pulsed 195 nm light. The exact wavelengths may differ slightly.

5.1 Final mixing stage (238 nm + 1080 nm → 195 nm)

This stage must sum 1080 nm light with 238 nm light to generate the 195 nm output. The 238 nm light is precious but the 1080 nm light is relatively cheap. Therefore we design this to use strong

1080 nm light to achieve near complete conversion of 238 nm to 195 nm. The relevant single pass mixing equation for one strong red wave is

$$\mathcal{P}_{193} = \frac{238}{193}\mathcal{P}_{238}\sin^2\left(\sqrt{\frac{\mathcal{P}_{1080}}{\mathcal{P}_\circ}}\frac{\pi}{2}\right). \tag{5.1}$$

$\mathcal{P}_\circ$ is a characteristic power that depends on the mixing parameters. It can be calculated using this equation under weak mixing using 2D-mix-LP. When the 1080 nm power equals this characteristic power, all of the 238 nm light is converted to 195 nm. For a 20 mm long CLBO crystal with a Rayleigh range of 20 mm for the two input beams, $\mathcal{P}_\circ = 260$ W. For a tighter focus this can be reduced to 115 W. If the ratio of Rayleigh range to crystal length is held constant, $\mathcal{P}_\circ$ scales as $1/L$, where L is the crystal length. Figure 5.2 shows the efficiency of 238 nm to 195 nm conversion as a function of the 1080 nm power. Operating at $_{1080} = \mathcal{P}_\circ$ makes the output power nearly immune to small fluctuations in the 1080 nm power and to fluctuations in length of the resonant cavity or the laser wavelength.

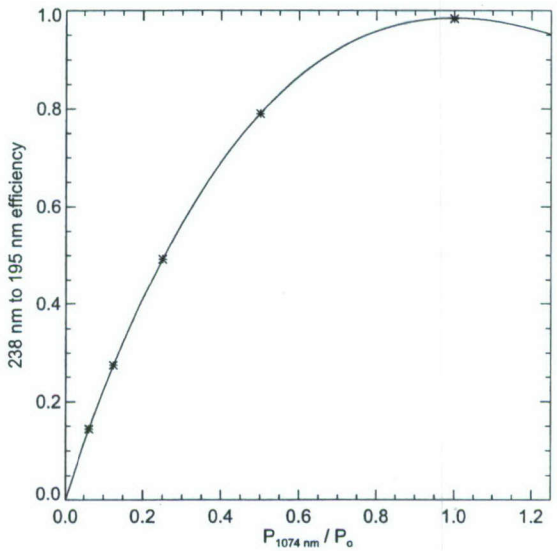

Figure 5.2: Conversion efficiency versus $\mathcal{P}/\mathcal{P}_\circ$. The symbols were calculated using 2D-cav-LP while the curve was calculated using Eq. (5.1) with a 1.5% reduction in maximum efficiency to account for the imperfect phase matching inherent in focused beam mixing.

Of course, 260 W seems rather high, but if the crystal is placed in a build up cavity that resonates the 1080 nm light, the input power is reduced substantially. For example, if the parasitic cavity losses for 1080 nm light are 3%, the input mirror reflectivity is set to 97% to impedence match the cavity, and this gives a factor of 33 power enhancement inside the cavity. Then the incident power can be 8 W rather than 260 W, and this is within reason for a narrow bandwidth fiber amplifier. I believe 3% loss is reasonable if the crystal can be AR coated. If it cannot be, the crystal faces can be cut at Brewster's angle. The loss of the 195 nm light at the exit face would be approximately 20%. If no coatings are used and normal faces are used the reflectivity per surface is 4% and the cavity

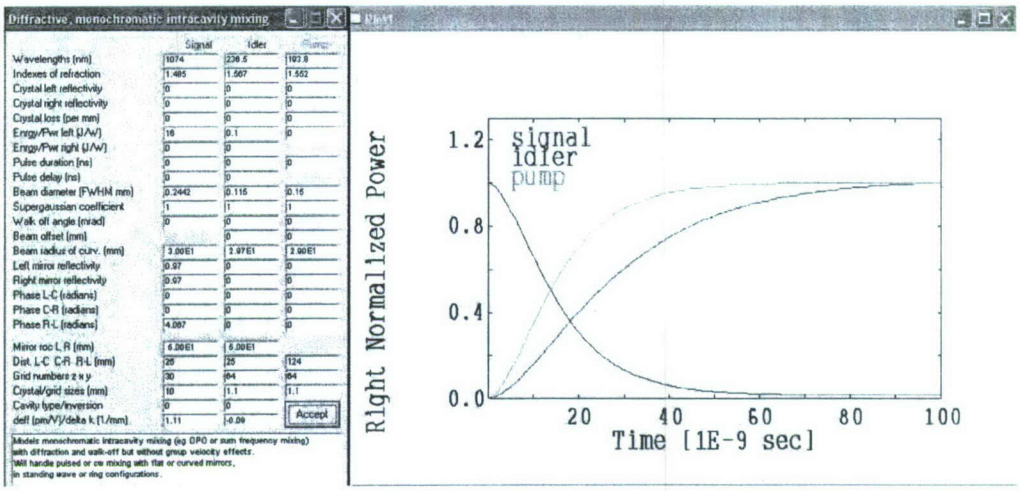

Figure 5.3: Modeled input/output powers for the final mixing stage. The run time of 100 ns is typical of the build up cavities used for all the build up cavities discussed for the conversion chain of this design.

enhancement is only 12.5, boosting the required input power 21 W. However, this could be halved by using a tighter focus, giving a requirement of 10 W input at 1080 nm, but with the tight focus thermal distortions might be a problem. The power levels, beam sizes, and wavelengths used for this stage are comparable to those used by Sakuma *et al.*[SDF+00, SAIO04] without any evidence of optical damage or thermal dephasing. Figure 5.3 shows the modeled performance of this stage.

5.2 Second SHG stage (476 nm → 238 nm)

This stage should use a cavity that resonates the 476 nm fundamental, but not the 238 nm second harmonic, to avoid reduction of the second harmonic power due to parasitic cavity losses. Resonating the fundamental also cleans up the 476 nm beam, and this helps maintain beam quality. This is equivalent to a doubly resonant cavity, because both fundamental waves are resonated, so high efficiency should be possible with only mW of fundamental power. Furthermore, because the power is low, it should be possible to use the tight focusing prescribed by the Boyd and Kleinman criterion, giving a Rayleigh range $z_R = 0.176L$ where L is the crystal length. $\mathcal{P}_\circ$ can be calculated using 2D-mix-LP, or if B&K focusing is used we can find it using

$$\mathcal{P}_\circ = S_\circ \frac{L\lambda_{SH}}{nh} \tag{5.2}$$

where h is the B&K focusing factor that is 1.068 for ideal focusing, and $S_\circ$ is a characteristic irradiance calculated by QMIX for each mixing process.

The optimum input mirror reflectivity and the conversion efficiency can be calculated using

$$R_F^{in} = 1 - \frac{1}{2}V - \frac{1}{2}\sqrt{V^2 + 4\frac{\mathcal{P}_F^{inc}}{\mathcal{P}_\circ}} \tag{5.3}$$

$$\mathcal{P}_{SH}^{em} = \mathcal{P}_F^{inc} \frac{T^{in} - V}{T_{in}(1 - V)} \tag{5.4}$$

where R^{in} is the optimum input mirror reflectivity, T^{in} is the input mirror transmission, V is the parasitic cavity loss for the fundamental, and $\mathcal{P}_{SH}^{em}$ is the emitted second harmonic power. For noncritical SHG of 476 nm light in a 10 mm long CLBO crystal $\mathcal{P}_\circ = 430$ W. If we assume $V = 0.02$, that is the parasitic loss of the fundamental is 2% per round trip of the cavity, and $\mathcal{P}_F^{inc} = 300$ mW, we find the ideal mirror reflectivity is

$$R_F^{in} = 0.962, \tag{5.5}$$

corresponding to an output power of

$$\mathcal{P}_{SH}^{em} = 145\text{mW}. \tag{5.6}$$

Figure 5.4 shows the input/output powers for this doubling stage generated by 2D-cav-LP. The result is in excellent agreement with the analytical expression.

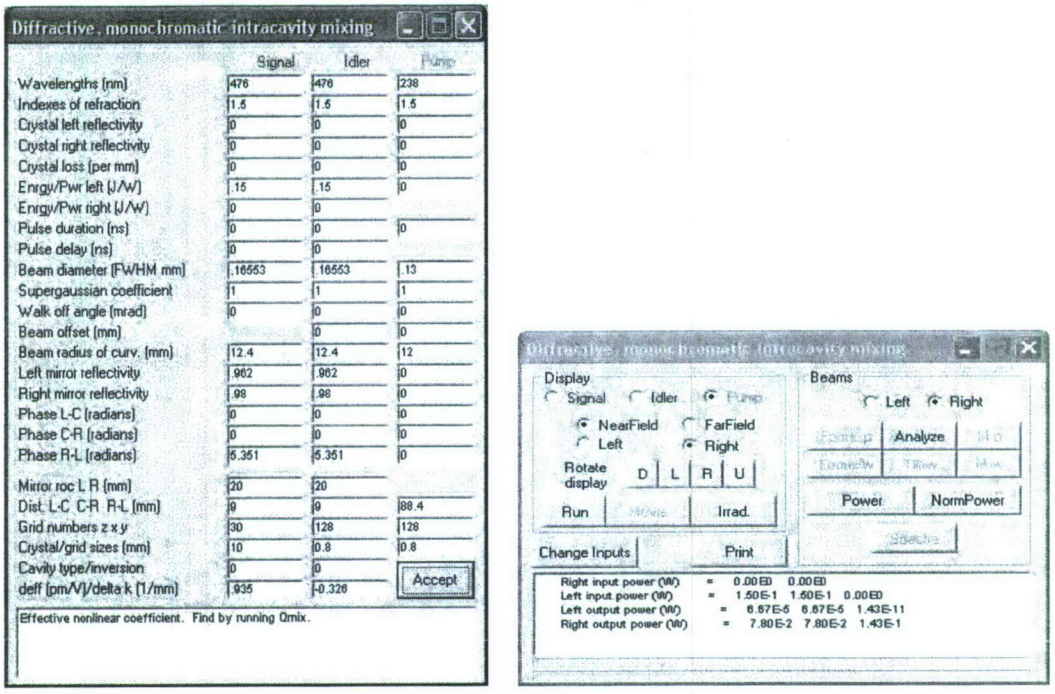

Figure 5.4: Model of SHG stage for generation of 140 mW of 238 nm light starting with 300 mW of 476 nm light.

5.3 First SHG stage (952 nm → 476 nm)

For this stage we chose periodically poled $LiTaO_3$ as the doubling crystal, and we focus the 952 nm fundamental weakly so the Rayleigh range is half the crystal length rather than the Boyd and Kleinman optimum $0.175L$. This should help avoid thermal and photorefractive problems. Using

a 10 mm crystal length with this focus, we find $\mathcal{P}_\circ = 110$ W by modeling with 2D-mix-LP and inserting the results in

$$\mathcal{P}_3^{em} = \frac{(\mathcal{P}_F^{inc})^2}{\mathcal{P}_\circ}. \tag{5.7}$$

We resonate only the 952 nm fundamental light, and assume it has a parasitic cavity loss of 2%. The equations for the optimum input mirror reflectivity and the output second harmonic power the same as above for the second SHG stage. If we start with 600 mW of 952 nm light the optimum value of R^{in} is 0.9155 and the predicted power at 476 nm is 467 mW. Figure 5.5 shows the input/output results of 2D-cav-LP that verify this efficiency.

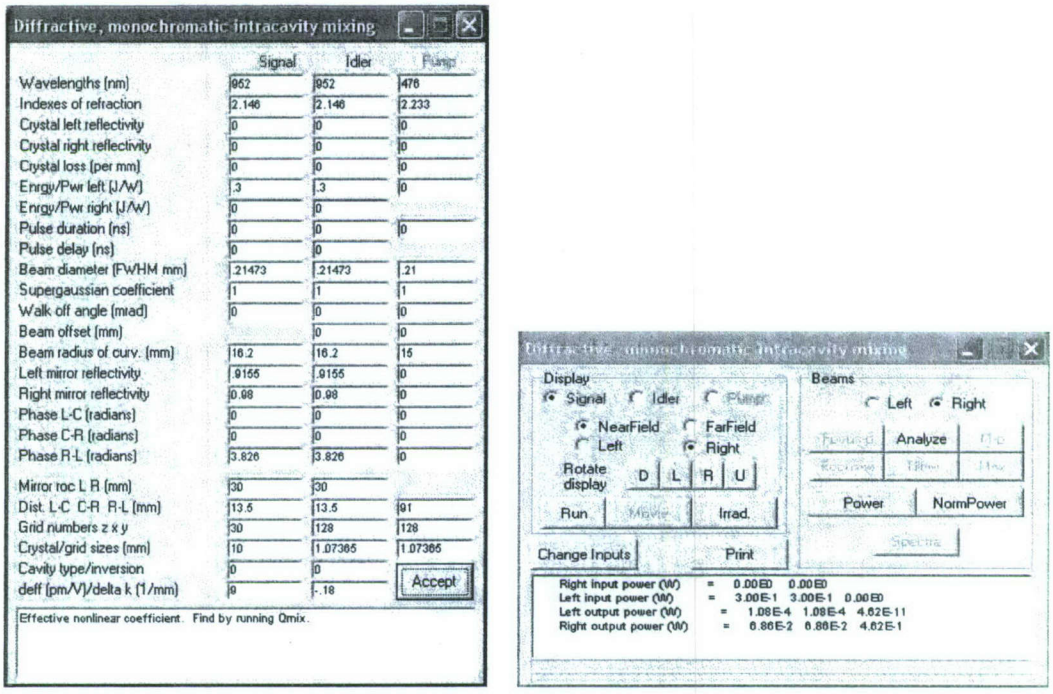

Figure 5.5: Model of SHG stage for generation of 467 mW of 476 nm light starting with 600 mW of 952 nm light.

5.4 OPO (540 nm → 952 nm + 1248 nm)

The design goal for this OPO is to generate 700 mW of 952 nm light starting with 2 W at 540 nm. A power of 2 W at 540 nm should avoid thermal and photo refractive problems in the 1080 nm SHG stage that preceeds the OPO as well as in the OPO. At this relatively low pump level a slightly pump-enhanced OPO makes sense, and that is what I model. However, a singly resonant OPO is also possible[HS07, HS06]. In addition to resonating the pump, either the signal or idler is resonated, but not both. Keeping the cavity singly resonant for the signal/idler avoids the nasty tuning problems of doubly resonant OPOs. The OPO cavity can be locked to the pump and the signal can be maintained on a single longitudinal mode using an intracavity etalon, or alternatively,

the cavity can be locked to a CW signal wavelength reference laser, and the pump laser can be locked to the cavity.

Resonating the 1248 nm beam gives higher efficiency for the 952 nm beam. However, we must watch for nonideal beam profiles for the unresonated 952 nm beam. This may not be an issue for this OPO because the 952 nm beam is the shorter wavelength of the two red beams, and this generally gives better beam profiles than when the longer wavelength is the unresonated wave. Nevertheless, we model both signal resonance and idler resonance for reference.

5.4.1 Resonating the 1248 nm beam

If the beam profiles are maintained in the mixing process, the minimum pump threshold for a pump enhanced OPO is

$$\mathcal{P}_3^{min} = V_1 V_3 \mathcal{P}_\circ \tag{5.8}$$

where V_3 and V_1 are the parasitic losses for the pump (540 nm) and resonated (1248 nm) waves, and $\mathcal{P}_\circ$ is defined by the low power, single pass mixing equation

$$\mathcal{P}_2 = \frac{\omega_2}{\omega_1}\frac{\mathcal{P}_1 \mathcal{P}_3}{\mathcal{P}_\circ}. \tag{5.9}$$

The efficiency of the unresonated 952 nm wave is

$$QE_2 = 1 - \frac{\mathcal{P}_3^{min}}{\mathcal{P}_3^{inc}} \tag{5.10}$$

which is achieved if the transmission of the pump beam and the 1248 nm beam have the optimum values given by

$$T_3^{in} = V_3 \frac{\mathcal{P}_3^{inc}}{\mathcal{P}_3^{min}} \tag{5.11}$$

$$T_3^{out} = V_3 \tag{5.12}$$

$$T_1^{in} = V_1. \tag{5.13}$$

Assuming 5% parasitic loss for the pump and resonated waves ($V_3 = V_1 = 0.05$), the minimum threshold is $\mathcal{P}_3^{min} = 2.5 \times 10^{-3}\, \mathcal{P}_\circ$. For a 20 mm long PPLT crystal and a Rayleigh range of 10 mm, $\mathcal{P}_\circ = 77$ W, the minimum pump threshold is $\mathcal{P}_3^{min} = 192$ mW, and the predicted output power at 952 nm is 1.02 W. Figure 5.6 shows the performance modeled using 2D-cav-LP. It agrees well with these predictions.

5.4.2 Resonating the 952 nm beam

Alternatively, we could resonate the 952 nm beam instead of the 1248 nm beam. This guarantees a stable, high quality transverse mode for the 952 nm beam, but the output power at 952 nm is reduced by the parasitic cavity losses. If we assume 5% parasitic loss for the 952 nm beam and the pump beam, $\mathcal{P}_\circ = 73$ W, and $\mathcal{P}_{min} = 182$ mW. The best efficiency for the 952 nm beam is

$$QE_1 = \left[1 - \sqrt{\frac{\mathcal{P}_3^{min}}{\mathcal{P}_3^{inc}}}\right]^2 \tag{5.14}$$

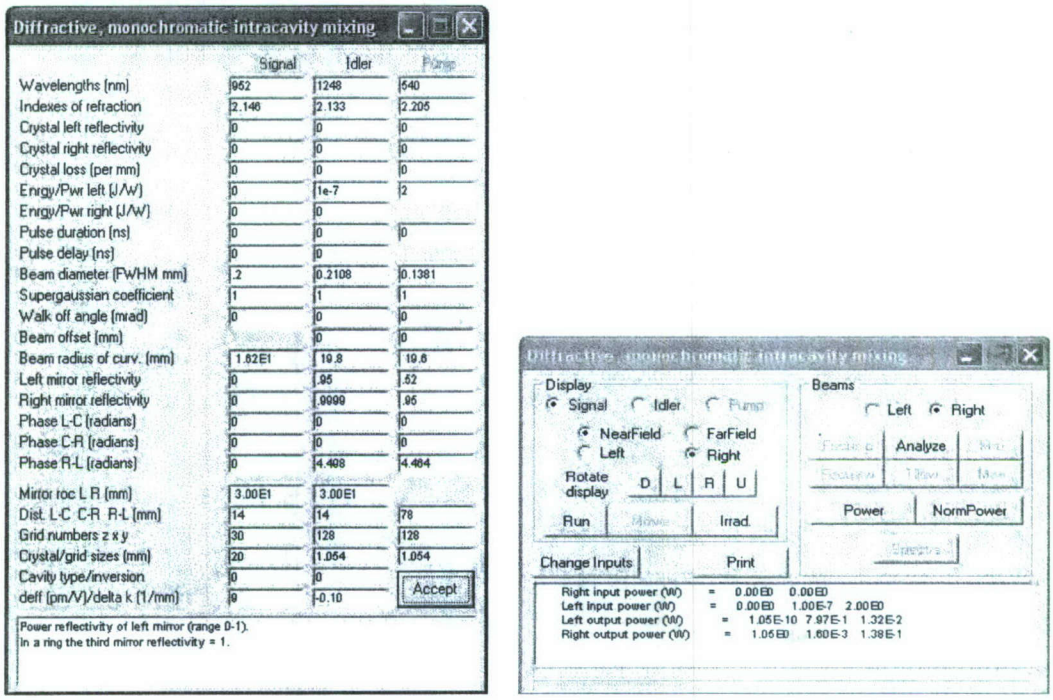

Figure 5.6: Model of the (540 nm → 952 nm + 1248 nm) OPO. 2 W of pump power generates 1 W of 952 nm light.

which requires

$$R_1^{out} = 1 - V_1 \left[\sqrt{\frac{\mathcal{P}_3^{inc}}{\mathcal{P}_3^{min}}} - 1 \right] \tag{5.15}$$

and

$$T_3^{in} = V_3 \sqrt{\frac{\mathcal{P}_3^{inc}}{\mathcal{P}_3^{min}}}. \tag{5.16}$$

These equations predict a 952 nm power of 0.55 W, only half that achieved by resonating the 1248 nm wave. Figure 5.7 shows the results of a 2D-cav-LP model run, indicating an output power of 0.570 W, in good agreement with the prediction.

5.5 Conclusions on a CW fiber-pumped system

The CW fiber-pumped system outlined seems feasible, although it is complex, requiring several stages that use build up cavities. A power of approximately 20 W from a 1080 nm fiber is sufficient to generate 100 mW at 195 nm. Roughly, 5 W is used to pump the OPO line that produces 100 mW of 238 nm light, and 10 W is used in the final mixing stage that sums 238 and 1080 nm beams. There are four and possibly five resonant cavities required, but these can all be based on a common design and can use common locking electronics. A high beam quality is maintained over the full

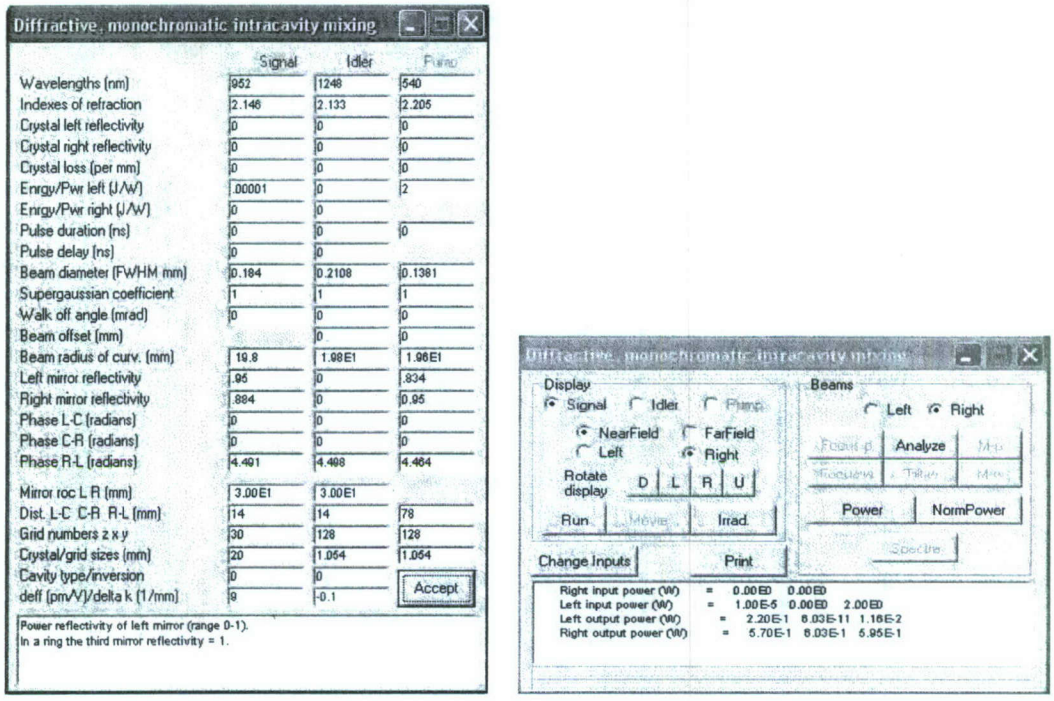

Figure 5.7: Model of the (540 nm → 952 nm + 1248 nm) OPO. 2 W of pump power generates 0.57 W of 952 nm light.

chain by the resonant cavities, so the 195 nm beam should be high beam quality, and it should also have a narrow spectral linewidth. Thermal and optical damage problems can arise in these devices, but I have attempted to keep power levels below those reported to cause problems.

Bibliography

[Agr89] G.P. Agrawal. *Nonlinear Fiber Optics.* Academic Press, 1989.

[CPTM00] P.A. Champert, S.V. Popov, J.R. Taylor, and J.P. Meyn. Efficient second-harmonic generation at 384 nm in periodically poled lithium tantalate by use of a visible Yb-Er-seeded fiber source. *Opt. Lett.*, 25(17):1252–1254, 2000.

[DDB+06] J.W. Dawson, A.D. Drobshoff, R.J. Beach, M.J. Messerly, S.A. Payne, A. Brown, D.M. Pennington, D.J. Bamford, S.J. Sharpe, and D.J. Cook. Multi-watt 589 nm fiber laser sorce. *SPIE*, 6102:6102F–1–9, 2006.

[GPT04] A.G. Getman, S.V. Popov, and J.R. Taylor. 7 W average power, high-beam-quality green generation in MgO-doped stoichiometric periodically poled lithium tantalate. *Appl. Phys. Lett.*, 85(15):3026–3028, 2004.

[GTB03] D.C. Gerstenberger, T.M. Trautmann, and M.S. Bowers. Noncritically phase-matched second-harmonic generation in cesium lithium borate. *Opt. Lett.*, 28(14):1242–1244, 2003.

[HHZ+03] J.-L. He, X.-P. Hu, S.-N. Zhu, Y.-Y. Zhu, and N.-B. Min. Efficient generation of red and blue light in a dual-structure periodically poled $LiTaO_3$ crystal. *Chin. Phys. Lett.*, 20(12):2175–2177, 2003.

[HLL+02] J.-L. He, J. Liu, G.-Z. Luo, Y.-L. Jia, J.-X. Du, C.-S. Guo, and S.-N. Zhu. Blue generation in a periodically poled $LiTaO_3$ by frequency tripling an 1342 nm Nd:$YV)_4$ laser. *Chin. Phys. Lett.*, 19(7):944–946, 2002.

[HPW94] G. Hollemann, E. Peik, and H. Walther. Frequency-stabilized diode-pumped Nd:YAG laser at 946 nm with harmonics at 473 and 237 nm. *Opt. Lett.*, 19(3):192–194, 1994.

[HPWL07] J. Hirohashi, V. Pasiskevicius, S. Wang, and F. Laurell. Picosecond blue-light-induced infrared absorption in single-domain and periodically poled ferroelectrics. *J. Appl. Phys.*, 101:033105–1–5, 2007.

[HS06] A. Henderson and R. Stafford. Low threshold, singly-resonant CW OPO pumped by an all-fiber pump source. *Opt. Exp.*, 14(2):767–772, 2006.

[HS07] A. Henderson and R. Stafford. Spectral broadening and stimulated Raman conversion in a continuous-wave optical parametric oscillator. *Opt. Lett.*, 32(10):1281–1283, 2007.

[HZZ+07] X.P. Hu, G. Zhao, C. Zhang, Z.D. Xie, J.L. He, and S.N. Zhu. High-power, blue-light generation in a dual-structure, periodically poled, stoichiometric $LiTaO_3$ crystal. *Appl. Phys. B*, 00:1–4, 2007.

[MLK+01] J.-P. Meyn, C. Laue, R. Knappe, R. Wallenstein, and M.M. Fejer. Fabrication of periodically poled lithium tantalate for UV generation with diode lasers. *Appl. Phys. B*, 73:111–114, 2001.

[SAIO04] J. Sakuma, Y. Asakawa, T. Imahoko, and M. Obara. Generation of all-solid-state, high-power continuous-wave 213-nm light based on sum-frequency mixing in $CsLiB_6O_{10}$. *Opt. Lett.*, 29(10):1096–1098, 2004.

[SDF+00] J. Sakuma, K. Deki, A. Finch, Y. Ohsako, and T. Yokota. All-solid-state, high-power, deep-UV laser system based on cascaded sum-frequency mixing in $CsLiB_6O_{10}$ crystals. *Appl. Opt.*, 39(30):5505–5511, 2000.

[SFF+08] P.E. Schrader, J.-P. Feve, R.L. Farrow, D.A.V. Kliner, R.L. Schmitt, and B.T. Do. Power scaling of fiber-based amplifiers seeded with microchip lasers. *SPIE*, xx:xx–xx, 2008.

[TKK07] S.V. Tovstonog, S. Kurimura, and K. Kitamura. High power continuous-wave green light generation by quasiphase matching in Mg stoichiometric lithium tantalate. *Appl. Phys. Lett.*, 90:051115–1–3, 2007.

[WAF02] P. Wessels, M. Auerbach, and C. Fallnich. Narrow-linewidth master oscillator fiber power amplifier system with very low amplified spontaneous emission. *Opt. Comm.*, 205:215–219, 2002.

[YKNK04] N.E. Yu, S. Kurimura, Y. Nomura, and K. Kitamura. Stable high-power green light generation with thermally conductive periodically poled stoichiometric lithium niobate. *Jap. J. Appl. Phys.*, 43(10A):L1265–L1267, 2004.

[ZLL+06] R. Zhou, E. Li, H. Li, P. Wang, and J. Yao. Continuous-wave, 15.2 W diode-end-pumped Nd:YAG laser operating at 946 nm. *Opt. Lett.*, 31(12):1869–1871, 2006.